

Optimization of Small-Molecule Inhibitors of Influenza Virus Polymerase: From Thiophene-3-Carboxamide to Polyamido Scaffolds

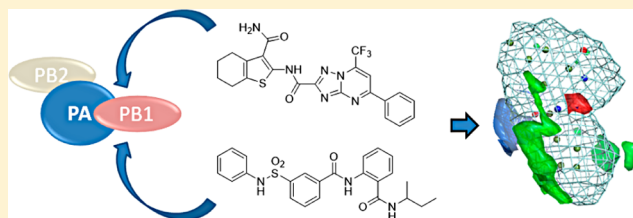
Susan Lepri,^{§,¶} Giulio Nannetti,^{⊥,¶} Giulia Muratore,[⊥] Gabriele Cruciani,[§] Renzo Ruzziconi,[§] Beatrice Mercorelli,[⊥] Giorgio Palù,[⊥] Arianna Loregian,^{*,⊥,||} and Laura Goracci^{*,§,||}

[§]Department of Chemistry, Biology and Biotechnology, University of Perugia, 06123 Perugia, Italy

[⊥]Department of Molecular Medicine, University of Padua, 35121 Padua, Italy

S Supporting Information

ABSTRACT: Influenza virus infections represent a serious concern to public health, being characterized by high morbidity and significant mortality. To date, compounds targeting the viral ion-channel M2 or the viral neuraminidase are the drugs available for treatment of influenza, but the emergence of drug-resistant viral mutants renders the search for novel targets and their possible inhibitors a major priority. Recently, we demonstrated that the viral RNA-dependent RNA polymerase (RdRP) complex can be an optimal target of protein–protein disruption by small molecules, with thiophene-3-carboxamide derivatives emerging as promising candidates for the development of new anti-influenza drugs with broad-spectrum activity. Here, we report a further dissection of the thiophene-3-carboxamide structure. By using a GRID molecular interaction field (MIF)-based scaffold-hopping approach, more potent and nontoxic polyamido derivatives were identified, highlighting a new space in the chemical variability of RdRP inhibitors. Finally, a possible pharmacophoric model highlighting the key features required for RdRP inhibition is proposed.



INTRODUCTION

Influenza A (FluA) and B (FluB) viruses are responsible for hundreds of thousands of deaths each year, especially among high-risk population groups (infants, elderly, people with immune deficiency).¹ The prophylactic, yearly reformulated vaccine and two classes of drugs are currently the only available anti-influenza therapeutic options.² The first class is represented by the M2 viral ion-channel inhibitors and includes the adamantanes (i.e., amantadine and rimantadine). The M2 inhibitors are only effective against FluA, and a significant increase of virus resistance to this class of compounds has been observed in recent years. Currently, all circulating FluA virus strains appear to be resistant to M2 inhibitors.^{3,4} The second class of antiviral compounds targets the viral neuraminidase (NA). NA inhibitors block the release of virions after budding from the host cell.^{5,6} Zanamivir was the first NA inhibitor commercially developed.⁷ It was discovered in 1989 using a target-guided design and exemplifies one of the first successful uses of this approach in drug discovery. The computational approach was based on the GRID force field, developed at the University of Oxford by Peter Goodford.⁸ The discovery of zanamivir was published in 1993 with more than a thousand citations to date. Although limited by poor bioavailability, zanamivir is still on the market, even though the orally active oseltamivir is usually preferred. Nowadays, NA inhibitors represent the only class of antiviral drugs to treat both FluA and FluB infections. However, resistance episodes were recently observed for oseltamivir in several Flu strains.^{3,9} For these reasons, increasing efforts have been devoted to the

identification of novel antiviral strategies.¹⁰ Recently, the viral polymerase attracted attention as a new target for the development of novel anti-influenza compounds.^{11–18} This protein is a heterotrimeric complex formed by the PB1, PB2, and PA subunits. The correct noncovalent assembly of the three subunits is essential for viral RNA synthesis.¹⁹ It is known that all three subunits, PB1, PB2, and PA, are necessary for both transcription and replication of the viral genome.^{20,21} PB1 possesses polymerase activity, PB2 is responsible for cap-binding of host cell pre-mRNAs, whereas PA contains the endonuclease domain and is implicated in RNA replication by cleaving capped host pre-mRNAs. The main advantage in exploiting the viral RNA polymerase as a target for drug design is that, in contrast to the viral glycoproteins, it is highly conserved among different viral strains,¹⁹ and thus RNA polymerase inhibitors are expected to possess a broad antiviral activity.²²

Just as the rational design of NA inhibitors became possible once the neuraminidase X-ray structure became available, today, the design of potential inhibitors of the influenza virus RNA polymerase is facilitated by the recent elucidation of its structure at atomic level.^{23–25} In particular, two recently published X-ray structures of a C-terminal domain of PA bound to an N-terminal peptide of PB1^{23,24} have clarified the molecular details of the PA–PB1 interaction: an N-terminal 3₁₀ helix from PB1 binds into a hydrophobic groove in the C-

Received: February 25, 2014

Published: May 1, 2014

terminus of PA, with relatively few residues driving the PA–PB1 binding. More recently, the PB1–PB2 interaction domain was also explored by X-ray crystallography.²⁵ Although the use of the PB1–PB2 interface as a target for the design of possible RdRP inhibitors is still under investigation,²⁶ the tailored design of small molecules that inhibit the formation of the PA–PB1 complex formation has already been demonstrated to be a promising strategy toward a new class of anti-influenza drugs.^{11–18} Attempts to inhibit the formation of the PA–PB1 complex using peptides have also been reported.^{27,28} However, whether it is better to use peptides or small molecules to inhibit protein–protein interaction is still a topic of much debate. On the one hand, peptides can better mimic the protein interaction showing high target selectivity and affinity.²⁹ On the other hand, small molecules usually possess better pharmacokinetic properties. Furthermore, there are only very few examples of unmodified peptides that have reached the market as drugs, due to their proteolytic instability or lack of cell permeation.

Recently, we reported an *in silico* screening of 3 million small molecule structures to search for inhibitors of the PA–PB1 interaction, using the X-ray structure of the PA subunit reported by He et al.²⁴ as a template.¹³ As a result, the *N*-(3-carbamoyl-5,6-dihydro-4*H*-cyclopenta[*b*]thiophen-2-yl)-7-(difluoromethyl)-5-phenylpyrazolo[1,5-*a*]pyrimidine-3-carboxamide, named as **1** in the present study (Figure 1, compound **5**

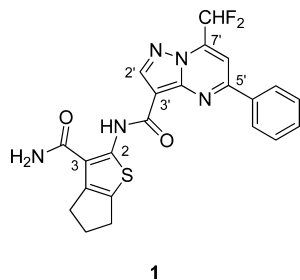


Figure 1. Chemical structure of compound **1**, an inhibitor of the PA–PB1 interaction.

in ref 12), was shown to inhibit the PA–PB1 complex formation *in vitro* (with an IC_{50} of $25.4 \pm 3.9 \mu M$) and to reduce the catalytic activity of the viral polymerase (with an IC_{50} of $31.4 \pm 4.2 \mu M$). In addition, compound **1** exhibited antiviral activity against FluA in infected cells at EC_{50} values around $100 \mu M$, without showing significant cytotoxicity ($CC_{50} > 250 \mu M$, evaluated in MDCK and 293T cell lines).¹³

Because of its promising potency and lack of cytotoxicity, we decided to give compound **1** further consideration.

In the present study, the optimization of compound **1** by using two different approaches is reported. A number of analogues of compound **1** were first synthesized to study the structure–antiviral activity relationship using a classical medicinal chemistry approach. In particular, the thiophene-3-carboxamide moiety was maintained, recently emerging as a promising scaffold for the design of RdRP inhibitors.¹⁶ Second, using compound **1** as a template, we applied a scaffold hopping approach to identify novel scaffolds for PA–PB1 complex inhibitors. The biological evaluation of the novel candidates is reported in terms of cytotoxicity, PA–PB1 binding disruption, and activity against Flu virus replication. Finally, a possible pharmacophore for PA–PB1 complex inhibitors is reported here for the first time.

RESULTS AND DISCUSSION

Design of Compound 1 Derivatives. Chemically, compound **1** is a pyrazolo[1,5-*a*]pyrimidine carrying a *N*-cyclopentathiophene carboxamide moiety at the C-3' position, a phenyl substituent at the C-5' position, and a difluoromethyl group at the C-7' position (Figure 1). In this study, the thiophenecarboxamide moiety was preserved since it was recently identified to be a promising scaffold for anti-Flu compounds.¹⁶ As a first attempt, the pyrazolo[1,5-*a*]pyrimidine (scaffold I, Table 1) was also maintained, while the difluoromethyl group, the cyclopentathiophene amide moiety, and the phenyl substituent at the C-5' position were modified (compounds **2–6**, Table 1). The selective incorporation of fluorine atom(s) or fluoroalkyl group(s) (such as CF_3 , CHF_2 , and CH_2F) into organic molecules has become a trend in life-sciences-related applications.^{30,31} Many studies have shown that a fluorine atom(s) or fluoroalkyl group(s) can bring several beneficial effects in bioactive molecules, such as the enhancement of metabolic stability, lipophilicity, bioavailability, and binding affinity.^{32–39} Among the fluoroalkyl groups, the difluoromethyl (CHF_2) group in compound **1** is of particular interest, because it is known to be isosteric and isopolar to a carbinol (CH_2OH) unit and, despite its lipophilic nature, can also act as a hydrogen bond donor.⁴⁰ By replacing the difluoromethyl group with the trifluoromethyl group (compounds **2**, **4–6**, Table 1), we wanted to investigate whether or not the hydrogen-bond donor capability of the CHF_2 group could be crucial in the interaction of compound **1** with PA.

Recent studies on new RdRP inhibitors bearing a cycloheptathiophene moiety revealed that the size of the aliphatic ring fused with thiophene was critical for the inhibitory effect.¹⁶ Therefore, we also tried to increase the size of the ring by replacing the cyclopentane with a cyclohexane ring (compounds **3–6**, Table 1).

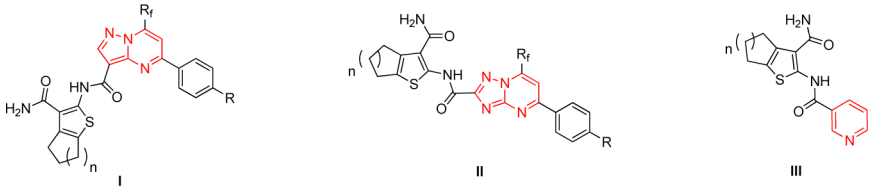
The last modification for scaffold I was the introduction of a hydrophobic or a hydrophilic substituent at the para-position of the phenyl ring (compounds **5** and **6** in Table 1, respectively).

The major structural modifications were performed by replacement of the pyrazolo[1,5-*a*]pyrimidine (scaffold I, Table 1) with a triazolopyrimidine or pyridine (scaffolds II and III in Table 1, respectively). The replacement of the carbon atom in the 3-position of the pyrazolo[1,5-*a*]pyrimidine with a nitrogen atom (as in scaffold II) forces the amidic bond to move from C-3' to C-2', leading to a more linear compound (**7**, Table 1).

Compound **8** was synthesized from scaffold III (Table 1). Its chemical structure shares some common features with a good inhibitor recently published,¹⁶ in which a 2-pyridyl-amide is bound to a cycloheptathiophene moiety at the C-2 position.

Scaffold Hopping Approach. A second strategy for the hit optimization was the use of compound **1** as a template for scaffold hopping, i.e., to search for new molecules endowed with similar chemical features but characterized by a different scaffold. This approach complements the classical structure–activity relationship (SAR) study reported in the previous section. Indeed, while structural modification on the same scaffold provides information on possible critical interactions for activity within a chemical series, the aim of a scaffold hopping approach is to move from a hit compound toward different scaffolds in the chemical space. Thus, if new active compounds with a different structure emerge, their common features can be related to activity.

Table 1. Summary of Activities of Synthesized Analogues of Compound 1 against FluA



comp	structure				ELISA PA–PB1 interaction assay	FluA minireplicon assay	FluA plaque reduction assay	Cytotoxicity (MTT) assay	
	scaffold	n	R _f	R				CC ₅₀ (μM) ^d	
					IC ₅₀ (μM) ^a	EC ₅₀ (μM) ^b	EC ₅₀ (μM) ^c	293T cells	MDCK cells
1	I	1	CHF ₂	H	27.2 ± 3.6	29.5 ± 5.4	75.5 ± 8.8	>250	>250
2	I	1	CF ₃	H	44.8 ± 3.3	27.5 ± 3.5	57.0 ± 15.5	>250	>250
3	I	2	CHF ₂	H	91.2 ± 7.4	94.2 ± 8.5	66.0 ± 8.5	>250	>250
4	I	2	CF ₃	H	120.4 ± 15.6	70.5 ± 6.6	>100	>250	>250
5	I	2	CF ₃	Me	43.0 ± 9.9	63.0 ± 9.9	100.7 ± 14.0	>250	>250
6	I	2	CF ₃	OMe	135.3 ± 14.2	ND	ND	40.4 ± 3.3	51.3 ± 3.1
7	II	2	CF ₃	H	7.5 ± 0.7	9.2 ± 2.3	23.7 ± 9.1	>250	>250
8	III	2			>200	ND	ND	>250	45.2 ± 3.1
9					35.1 ± 4.3	ND	ND	12.4 ± 2.3	18.3 ± 2.5
10					30.5 ± 6.2	45.9 ± 4.4	18.7 ± 3.8	>250	>250
11					>200	ND	ND	30.1 ± 4.1	20.2 ± 3.3
12					>200	>100	>100	>250	>250
PB1 _{1–15} -Tat peptide					37.2 ± 5.6	20.9 ± 6.7	50.5 ± 13.8	>250	>250
RBV					ND	24.9 ± 5.1	15.6 ± 6.3	>250	>250

^aActivity of the compounds in ELISA PA–PB1 interaction assays. The IC₅₀ value represents the compound concentration that reduces by 50% the interaction between PA and PB1. ^bActivity of the compounds in minireplicon assays. The EC₅₀ value represents the compound concentration that reduces by 50% the catalytic activity of FluA polymerase. ^cActivity of the compounds in plaque reduction assays with the FluA PR8 strain. The EC₅₀ value represents the compound concentration that inhibits 50% of plaque formation. ^dActivity of the compounds in MTT assays. The CC₅₀ value represents the compound concentration that causes a decrease of cell viability of 50%. All the reported values represent the means ± SD of data derived from at least three independent experiments in duplicate. ND: not determined.

As mentioned above, a structure-based virtual screening on 3 million compounds using the X-ray structure of the PA subunit as a template was previously used to identify 293 possible PA–PB1 complex inhibitors. Of the 293 hits, only 32 compounds (including our hit compound) were acquired and tested.¹³ In this study, starting with compound 1 as a template, we screened the 293 compounds using the FLAP algorithm⁴¹ to evaluate their similarity based on the GRID molecular interaction fields (MIFs).^{8,42} The subset of 293 compounds were thus ranked by their similarity to the template. On the basis of this similarity scoring and taking into consideration their availability, cost, and druggability, four commercially available compounds (9–12 in Figure 2) were acquired and tested. Interestingly none of them possess a thiophene-3-carboxamide scaffold.

Chemistry. Synthesis of 2-Aminothiophene-3-[substituted]carboxamide Compounds. The synthesis of compound 1 and its analogues 2–8 is illustrated in Scheme 1. Knoevenagel condensation of cyanoacetamide with cyclopentanone or cyclohexanone followed by sulfur-promoted cyclization gave the suitable thiophene carboxamide derivatives 13a–b, respectively.⁴³ The final amidopyrazoles 1–8 were obtained by oxalyl chloride-promoted condensation of amino-thiophenes 13a–b with the appropriate carboxylic acid, obtained by alkaline hydrolysis of the respective ethyl esters. The esters for the synthesis of products 5–8 were acquired from SPECS (www.specs.net), whereas the esters 14a–b were prepared by condensing the commercially available ethyl 3-amino-1H-pyrazole-4-carboxylate with fluorinated 1,3-diones⁴⁴ (Scheme 2). The triazole derivative 7 and the nicotinamide 8

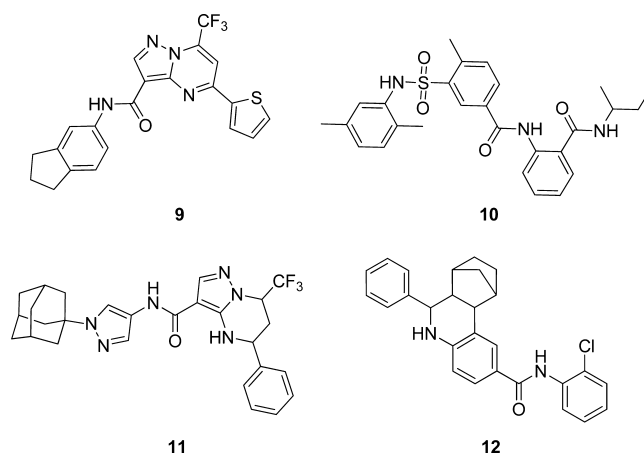
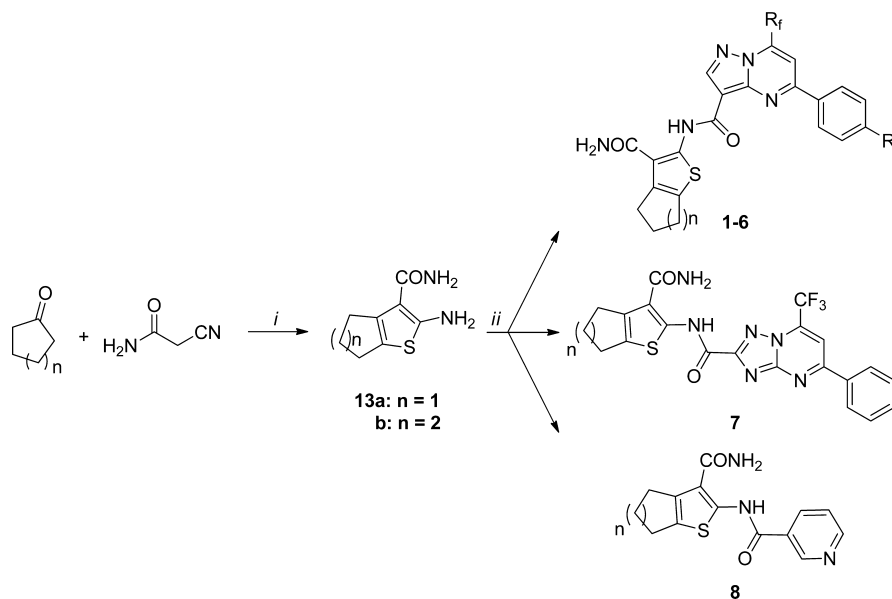


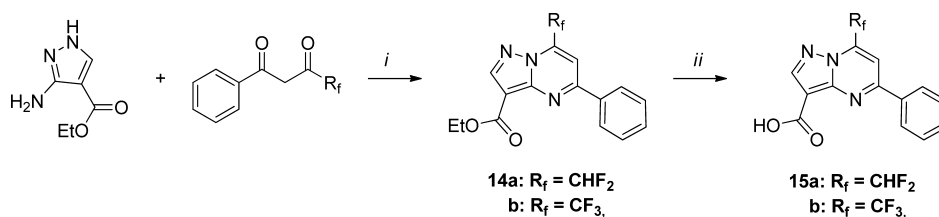
Figure 2. Structures of four analogues of compound 1, according to the FLAP similarity score.

were analogously prepared by coupling amino-thiophene 13b either with the chloride of the commercially available 5-phenyl-7-(trifluoromethyl)-[1,2,4]triazolo[1,5-a]pyrimidine-2-carboxylic acid or with nicotinoyl chloride, respectively.

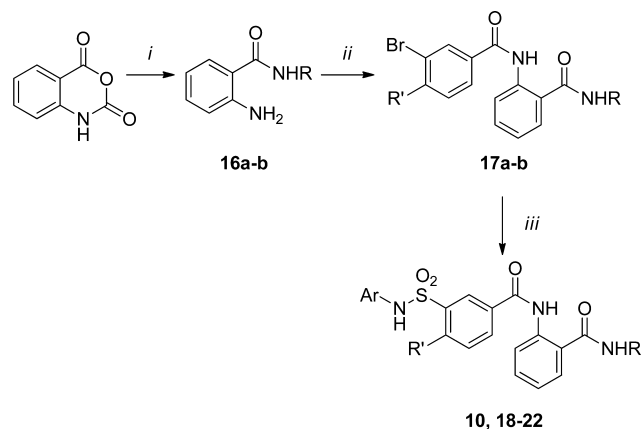
Synthesis of Polyamido Derivatives. A number of derivatives of compound 10 were also synthesized. The polyamido-sulfonamides 18–22 were prepared according to literature procedures or their modification (Scheme 3). Thus, the nucleophilic attack of either *sec*-butylamine or aniline at C-4 of isatoic anhydride, followed by the elimination of carbon

Scheme 1^a

^aReagents and conditions: (i) S_8 , morpholine, EtOH, 60 °C;⁴³ (ii) 1. Suitable carboxylic acid (see Experimental Section), oxalyl chloride, DCM, DMF cat.; 2. Pyridine, DCM. For R and R_f definition see Table 1.

Scheme 2^a

^aReagents and conditions: (i) AcOH reflux;⁴⁴ (ii) NaOH, EtOH, H_2O .

Scheme 3^a

^aReagents and conditions: (i) *sec*-butylamine (for **16a**) or aniline (for **16b**), DMF, 100 °C;⁴⁵ (ii) 3-bromobenzoyl chloride (for **17a**) or 3-bromo-4-methylbenzoyl chloride (for **17b-c**) Et_3N , toluene, reflux; (iii) 1. *n*-BuLi, −78 °C, THF; 2. SO_2 , −60 °C, THF;⁴⁷ 3. NCS, DCM; 4. $ArNH_2$, Et_3N , acetone, 50 °C.⁴⁸ For Ar see Table 2.

dioxide from the carbamic acid intermediate, gave the anthranilamides **16a-b**, respectively, in excellent yield.^{45,46}

The condensation of the anthranilamides **16a-b** with 4-substituted 3-bromobenzoyl chloride in refluxing toluene, in the

presence of triethylamine, afforded the bisamide **17a-c**. Butyllithium-promoted bromine–lithium exchange in THF at −78 °C, followed by addition of sulfur dioxide at −60 °C, converted the bromo derivatives **17a-c** in the corresponding lithium sulfinate.⁴⁶ The latter were treated with *N*-chlorosuccinimide to give the expected sulfonyl chlorides, which were smoothly converted into the target sulfonamide **10** and **18–22** in 20–25% overall yield by reaction with the suitable amine in acetone at 50 °C.⁴⁸

Biological Evaluation. Our hit compound **1**, previously tested as provided from the vendor,¹³ was synthesized and retested, giving comparable results (Table 1).

The synthesized compounds **2–8** and the acquired compounds **9–12** were tested in ELISA to determine their inhibitory activity on PA–PB1 interaction. The PB1(1–15)–Tat peptide¹³ was used as a positive control. In addition, we evaluated the ability of the compounds to inhibit the activity of FluA RNA polymerase by a minireplicon assay in transfected HEK 293T cells,⁴⁹ while the antiviral activity in FluA virus-infected MDCK cells was evaluated by plaque reduction assays (PRA) using the A/PR/8/34 (PR8) strain. In these assays, ribavirin (RBV), a known inhibitor of RNA viruses polymerase,⁵⁰ was used as a positive control. Moreover, MTT cytotoxicity assays in MDCK and HEK293T cell lines using RBV as a reference compound were also performed to exclude

Table 2. Summary of Activities of Analogues of Compound 10 against FluA Virus

Comp.	Structure			ELISA PA-PB1 Interaction Assay IC ₅₀ (μM) ^a	FluA Minireplicon Assay EC ₅₀ (μM) ^b	FluA Plaque Reduction Assay EC ₅₀ (μM) ^c	Cytotoxicity (MTT) Assay CC ₅₀ (μM) ^d	
	R	R'	Ar				293T cells	MCDK cells
10	<i>sec</i> -Bu	Me		30.5 ± 6.2	45.9 ± 4.4	18.7 ± 3.8	>250	>250
18	<i>sec</i> -Bu	H		84.0 ± 5.6	25.7 ± 6.2	35.2 ± 10.3	>250	>250
19	<i>sec</i> -Bu	H		9.2 ± 1.5	17.2 ± 1.3	30.5 ± 4.4	>250	>250
20	<i>sec</i> -Bu	Me		>200	>100	>100	>250	>250
21	Ph	Me		91.9 ± 16.7	>100	24.7 ± 7.8	>250	70.3 ± 5.5
22	<i>sec</i> -Bu	H		>200	82.6 ± 5.7	>100	>250	>250
PB1 ₁₋₁₅ -Tat peptide				37.2 ± 5.6	20.9 ± 6.7	50.5 ± 13.8	>250	>250
RBV				ND	24.9 ± 5.1	15.6 ± 6.3	>250	>250

^aActivity of the compounds in ELISA PA–PB1 interaction assays. The IC₅₀ value represents the compound concentration that reduces the interaction between PA and PB1 by 50%. ^bActivity of the compounds in minireplicon assays. The EC₅₀ value represents the compound concentration that reduces the catalytic activity of FluA polymerase by 50%. ^cActivity of the compounds in plaque reduction assays with the FluA PR8 strain. The EC₅₀ value represents the compound concentration that inhibits 50% of plaque formation. ^dActivity of the compounds in MTT assays. The CC₅₀ value represents the compound concentration that causes a decrease of cell viability of 50%. All the reported values represent the means ± SD of data derived from at least three independent experiments in duplicate.

cytotoxic compounds. Antiviral activity and toxicity data for all the tested compounds are reported in Table 1.

Modifications made using scaffold I (compounds 2–6) did not give any significant improvement in the antiviral activity. However, a comparison of the results for 1 and 2, differing in the fluorinated substituent only, reveals that the H-bond donor capability of the CHF₂ moiety seems not to be critical for inhibition. On the other hand, the replacement of the cyclopentathiophene moiety of compound 1 with the cyclohexathiophene moiety to give compound 3 induced a 3-fold increase of the IC₅₀ value in the ELISA and of the EC₅₀ value in the FluA minireplicon assay, although the activity of compound 3 against FluA replication is very similar to those of compounds 1 and 2. Surprisingly, the additional substitution of CHF₂ with CF₃ (compound 4) led to a decreased activity in all the tests performed. When a methyl group was added in the para-position of the phenyl ring of compound 4 to give compound 5, a decrease of the IC₅₀ value in the ELISA and the EC₅₀ value in

the FluA minireplicon assay was observed. The inhibitory efficacy in PRA was also slightly improved, even though compound 5 resulted to be a weaker inhibitor with respect to the hit compound. This finding is in agreement with our previous results,^{13,16} indicating that hydrophobic interactions are favorable in designing RdRP inhibitors. When a polar substituent such as a methoxy group was introduced instead of a methyl group to give compound 6, a less active compound in the ELISA assay was obtained. This compound also resulted to be toxic in cell-based assays. Compound 6 appeared to be the only cytotoxic compound in the scaffold I series.

Even though the optimization of the scaffold I did not bring successful results, the replacement of the pyrazolo[1,5-*a*]pyrimidine with a triazolopyrimidine (scaffold II) to give compound 7 in Table 1 proved to be very effective. Indeed, compound 7, which bears the CF₃ substituent and cyclohexane, resulted to be about 3-fold more efficient than compound 1 in inhibiting both PA–PB1 complex formation and viral

Table 3. Evaluation of Broad-Spectrum Activities of Most Active Compounds

compound	PRA vs FluA (EC_{50} , μ M) ^a				PRA vs FluB (EC_{50} , μ M) ^a	
	H1N1			H3N2		
	A/Solomon Island/3/06	A/Padova/30/11	A/Parma/24/09 (oseltamivir-resistant)	A/WSN/67/05	B/Lee/40	B/Malaysia/2506/04
1	>100	>100	95.5 \pm 5.6	>100	>100	>100
7	23.3 \pm 3.0	20.6 \pm 2.8	22.9 \pm 1.5	20.0 \pm 2.3	33.5 \pm 4.2	25.9 \pm 1.8
10	17.5 \pm 2.6	22.6 \pm 5.3	25.0 \pm 2.6	15.9 \pm 3.2	21.8 \pm 1.4	29.6 \pm 4.0
18	16.5 \pm 1.7	16.7 \pm 4.2	22.1 \pm 2.1	10.8 \pm 2.1	15.5 \pm 2.1	19.8 \pm 4.2
19	22.5 \pm 3.5	37.6 \pm 6.6	43.0 \pm 3.6	23.5 \pm 2.8	25.5 \pm 3.7	26.3 \pm 5.5

^aActivity of the compounds in plaque reduction assays with the different FluA and FluB strains. The EC_{50} value represents the compound concentration that inhibits 50% of plaque formation. All the reported values represent the means \pm SD of data derived from at least three independent experiments in duplicate.

replication. Purification difficulties were encountered during the synthesis of the cyclopentane analogue, and thus further investigation of this scaffold would require an optimization of the reaction conditions. The replacement of the pyrazolo[1,5-*a*]pyrimidine with a pyridine to give scaffold III in Table 1 led to a cytotoxic compound (compound 8) with no activity according to the ELISA.

Concerning the four compounds acquired following the scaffold hopping approach, the polyamido derivative 10 was found to be a good RdRP inhibitor. Indeed, compound 10 not only exhibited an inhibitory activity against the PA–PB1 interaction comparable to that of the hit compound but also proved to be 4-fold more potent than compound 1 in blocking FluA replication. Of the other three acquired compounds (9, 11, 12), compounds 9 and 11 resulted to be cytotoxic, although an IC_{50} of $35.1 \pm 4.3 \mu$ M was obtained for compound 9 in the ELISA assays. Thus, these compounds were not further investigated. Compound 12 was found to be not cytotoxic but also inactive. To further investigate the new polyamido scaffold, compound 10 and five analogues were synthesized. Tests on the resynthesized compound 10 gave comparable inhibitory effects to those obtained using the commercial sample both in ELISA (IC_{50} values of 28.7μ M and 30.5μ M, respectively) and in PRA (EC_{50} values of 19.3μ M and 18.7μ M, respectively).

The derivatives of compound 10 were aimed at tuning the hydrophobicity and their size. Compounds 18 and 19, which differ from the reference compound for the lack of one or all methyl substituents, respectively, were synthesized first. Methyl groups are not likely to be involved in specific interaction with protein residues, but enhancing the overall hydrophobicity could play a role in RdRP inhibitory efficacy, since it is known that the PA cavity is mainly hydrophobic.^{13,16,51} Compounds 20 and 21 were then synthesized by adding an additional aromatic ring to the two edges of compound 10. These compounds served to preliminary investigate whether larger and more hydrophobic compounds could display a similar inhibitory activity. To mimic a “peptide-like” feature, an amide linkage was used, which was typical of the polyamido scaffold of compound 10. Finally, compound 22 was synthesized as an attempt to explore the effect of the introduction of polar substituents. The structures and biological data for the five polyamido derivatives are reported in Table 2.

Removal of one (18) or all (19) methyl groups gave results comparable to the lead 10, so we assumed that their role was not crucial for preservation of antiviral activity. However, compound 19 resulted in the most efficient in inhibiting the PA–PB1 interaction, giving an IC_{50} value of $9.2 \pm 1.5 \mu$ M in the ELISA.

Addition of a further hydrophobic moiety on the sulfonamide part, as in compound 20, did not affect cytotoxicity, but had a detrimental effect on the antiviral activity. On the other hand, replacement of the *sec*-butyl group in the terminal amido moiety with a phenyl ring, as in compound 21, resulted in toxicity in MCDK cells. This compound is only modestly active in ELISA; thus its good antiviral activity in PRA could be due to its toxicity profile. Finally, compound 22, which held a hydroxyl group in para-position of sulfonamide portion, showed a dramatic decrease in activity.

To test the specificity of the inhibitory activity, the four most active compounds (compounds 7, 10, 18, and 19) and hit compound 1 as a reference were tested by ELISA for inhibition of an unrelated protein–protein interaction, i.e., the interaction between the UL54 and UL44 subunits of human cytomegalovirus (HCMV) DNA polymerase complex as previously described.^{52,53} None of the tested compounds exhibited a dose-dependent inhibitory activity up to a concentration of 200μ M. In contrast, compound AL5, previously shown to inhibit the interactions between the HCMV DNA polymerase subunits,⁵³ did interfere with UL54–UL44 binding (see Figure S1 in the Supporting Information).

The antiviral effect of the four most active compounds 7, 10, 18, and 19 was finally investigated against a number of clinical isolates of FluA other than PR8, of both H1N1 and H3N2 subtypes, including a swine-derived pandemic strain and an oseltamivir-resistant virus. In addition, the same compounds were also tested for their ability to inhibit the replication of two FluB strains (B/Lee/40 and B/Malaysia/2506/04). The hit compound 1 was also included as a reference compound. The biological data for the evaluation of broad-spectrum activity are reported in Table 3.

Compounds 7, 10, 18, and 19 displayed a similar antiviral activity against all FluA and FluB strains, with EC_{50} values ranging from 10.8 to 43.0μ M and significantly higher than those of compound 1, confirming the successful optimization of the hit compound.

Preliminary ADME studies (water solubility, permeability, and metabolic stability) were performed for compounds 7 and 19, which were the most promising compounds. Methods for these studies are reported in the Supporting Information. Concerning water solubility, compounds 7 and 19 showed a solubility of 2.4 and 1.0μ g/mL, respectively, measured by NMR as previously reported.⁵⁴

A preliminary PAMPA permeability assay⁵⁵ was also performed, with compound 19 resulting to be in the range of medium/high permeability, while compound 7 fell in the “low permeability” class. Finally, metabolic stability was evaluated in HLM after 30 min incubation. Compound 7 was metabolically

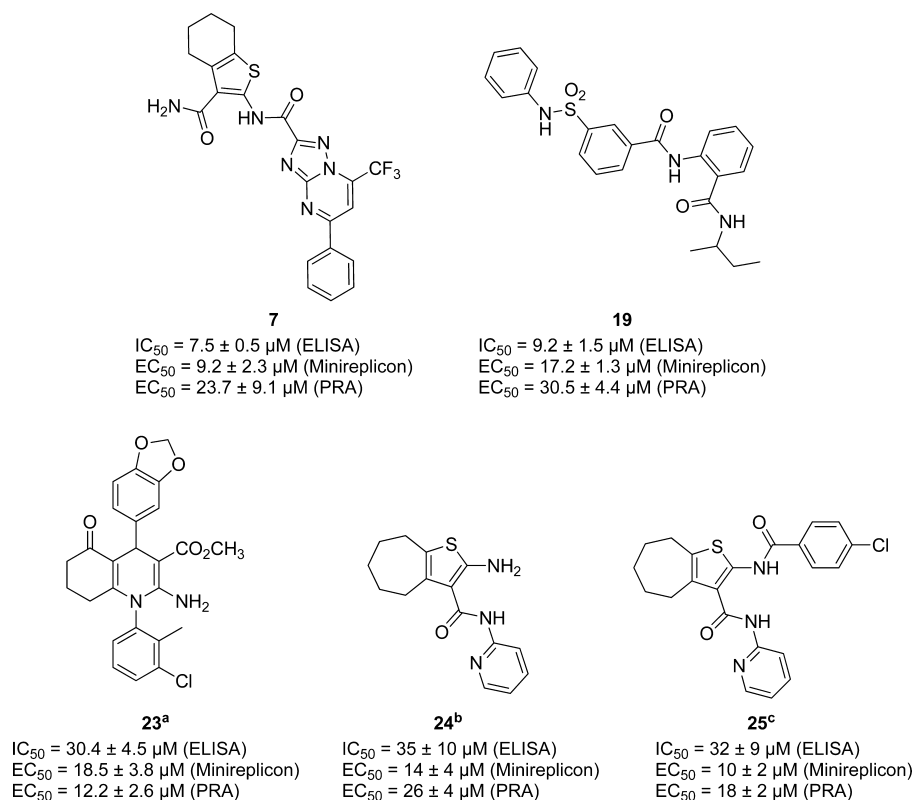


Figure 3. Structure of the five RdRP inhibitors used for pharmacophore generation. ^aCompound **1** in ref 13; ^bcompound **19** in ref 16; ^ccompound **6** in ref 16.

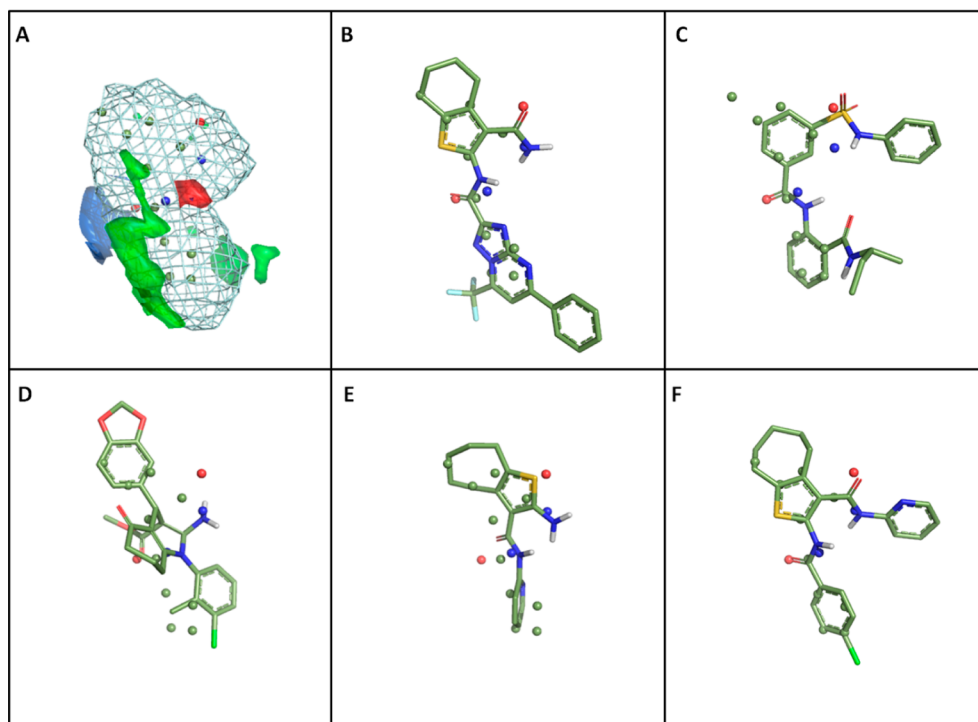


Figure 4. Pharmacophore for RdRP inhibitors targeting the PA–PB1 complex generated by FLAP. (A) Structure of the pharmacophore. The shape is reported as a wireframe surface, while the pharmacophoric points and GRID MIFs are reported as solid spheres and surfaces, respectively. Color-code: green = hydrophobic; red = H-bond acceptor; blue = H-bond donor. (B–F) compounds **7**, **19**, **23**, **24**, **25** aligned to the pharmacophore, respectively.

stable in HLM, while compound **19** underwent through aromatic hydroxylation at the benzenesulfonamide moiety to

give the monohydroxylated metabolite. After 30 min, substrate was at 50% abundance. The metabolic stability of compound **1**

was also measured, and aliphatic hydroxylation at the cyclopentane ring was observed, with compound **1** reduced to 37%, highlighting the better stability of compounds **19** and **7** with respect to the hit compound. Although the reported ADME profile is still very preliminary, it suggests that both compounds are too lipophilic, and further lead optimization will be aimed at finding the best compromise between lipophilicity (which is important for activity) and solubility.

Pharmacophore Generation. Our recent studies, aimed at discovering new small-molecule antiviral compounds targeting the PA–PB1 subunit interaction of the viral RdRP, led to the identification of five compounds that possess very different chemical structures but similar inhibitory activity against the replication of FluA and FluB. Compounds **7** and **19** were found to be the most potent RdRP inhibitors. Three other compounds were previously reported by some of us to be active against the influenza polymerase complex.^{13,16} The chemical structures of the five compounds are reported in Figure 3. When a number of active compounds with different scaffolds are identified, the most natural step to advance their improvement is to attempt to generate a possible pharmacophore. A pharmacophoric model was therefore generated by alignment of the five compounds using the FLAP_{pharm} algorithm.⁵⁶

The pharmacophoric model is reported in Figure 4A, while the structures of the five compounds aligned to the pharmacophore are reported in Figure 4B–F. As shown in Figure 4A, a pharmacophore generated by FLAP is composed of three entities: a shape (the wireframe surface), a number of common atomic features indicating pharmacophoric points (the spheres), and a number of regions (the solid surfaces) indicating the most conserved GRID MIFs. The latter point is very important since GRID MIFs provide information on the possible interaction of a ligand with a target. Conserved GRID MIFs among aligned active compounds are therefore likely to be related to the activity. In Figure 4, the green MIFs are related to hydrophobic interactions, while blue and red MIFs refer to H-bond donor and H-bond acceptor interactions, respectively. The same color-code is also used for the pharmacophoric points.

According to the pharmacophore GRID MIFs, extended and quite planar hydrophobic moieties represent a common feature among the RdRP inhibitors (green solid surface in Figure 4A). In addition, one H-bond donor and one H-bond acceptor MIF emerged upon alignment of the five compounds (blue and red solid surfaces in Figure 4A, respectively). By observing the correspondence of the GRID MIFs, the pharmacophoric points (spheres), and the chemical structures of the aligned compounds, it becomes clear that in all compounds a carbonyl moiety is responsible for the H-bond donor MIF, acting as a H-bond acceptor group, while the red MIFs are generated by an NH group acting as a H-bond donor. In this case, the nature of the NH moiety seems to be variable, ranging from amines, anilines, amides, and sulfonamides. To further validate our pharmacophoric hypothesis, five other recently published RdRP inhibitors targeting the PA–PB1 complex were selected and aligned on the pharmacophore. Among them, three inhibitors were benzofurazan derivatives (compounds **8c** and **47e** in ref 17 and compound **7e** in ref 15), and the remaining two compounds were 3-cyano-4,6-diphenyl pyridine derivatives (compounds **11** and **12** in ref 18). Compounds **11**, **12**, and **8c** were able to fit all the pharmacophoric regions previously described, while compounds **47e** and **7e** only lack the H-bond

donor group to match the GRID acceptor field (see Figure S2 in the Supporting Information). This result, in addition to the variability of the NH groups previously discussed, suggests that the H-bond acceptor GRID MIF region could be less critical for binding.

CONCLUSIONS

In recent years, the viral RdRP has proved to be an attractive target in the design of small molecules capable of inhibiting influenza virus replication. A few RdRP inhibitors have been published so far, and their antiviral activity is sometimes associated with cytotoxic effects.^{15,17} The aim of this study was to further dissect the chemical space of the RdRP inhibitors targeting the PA–PB1 complex. The previously published compound **1** was selected as a hit compound for further optimization by two complementary approaches: (1) the design and the synthesis of derivatives of compound **1**, to investigate the structural features that might be responsible for PA–PB1 complex disruption; (2) a scaffold hopping approach to identify novel scaffolds for PA–PB1 complex inhibitors. In the modulation of the chemical structure of compound **1**, the thiophene-3-carboxamide moiety, which emerged as a favorable scaffold in the design of RdRP inhibitors,¹⁶ was always preserved. However, when the pyrazolo[1,5-*a*]pyrimidine was replaced with a triazolopyrimidine to give compound **7**, a 3-fold more potent PA–PB1 inhibitor was obtained with respect to compound **1**, inhibiting the physical interaction between the two viral subunits with an IC₅₀ value of $7.5 \pm 0.7 \mu\text{M}$. This finding suggests that the synthesis of new derivatives having a more linear shape might be helpful to improve the inhibitory effect. As a result of the scaffold hopping approach, we identified the sulphonamide compound **10**, which was acquired and assayed. Despite the significantly different polyamido scaffold, compound **10** produced a good RdRP inhibitory effect targeting the PA–PB1 complex. The synthesis of the slightly different compound **19** led to an inhibitory activity comparable to that of compound **7**. Both compounds **7** and **19** were found to be not cytotoxic in the two cell lines used for testing, and they were also able to inhibit a number of FluA and FluB strains.

The discovery of two very different scaffolds with similar activities prompted us to generate a pharmacophoric model by also taking into consideration three other recently published RdRP inhibitors that have been proven to be active against FluA and FluB. On the basis of this model, all the selected active compounds were shown to possess an extended and quite planar hydrophobic moiety. In addition, the alignment of the molecular structures revealed that they have a common carbonyl group which is able to act as a H-bond acceptor, and in the opposite site an NH group of varying chemical nature which is able to act as a H-bond donating group. The proposed pharmacophore could be useful to design novel RdRP inhibitors, focusing the attention on similar interaction capabilities rather than on similar scaffolds.

EXPERIMENTAL SECTION

Computational Methods. The search for novel scaffolds for RdRP inhibitors and pharmacophore generation were performed using the FLAP algorithm.^{41,56} The FLAP software is developed and licensed by Molecular Discovery Ltd. (www.moldiscovery.com). In the scaffold hopping study, a database containing the best 293 hits previously selected as possible PA–PB1 interaction inhibitors¹³ was prepared. All protomeric forms in at least 20% abundance at pH 7.4 were generated

for each compound using the MoKa algorithm.^{57,58} A number of 50 conformers for each protomer was also generated to mimic flexibility. Then a ligand-based virtual screening was performed using compound **1** as a template. Thus, in this study FLAP algorithm was not used to perform *de novo* virtual screening but only to rescore the best hits found by a structure-based approach¹³ for their similarity to our hit compound. The 293 candidates were ranked by the GloB-Sum descriptor, and four compounds having a similarity score >1.5 and different scaffolds were selected. Their availability, cost, and druggability were also taken into consideration. Chemical structures for the 293 compounds and their FLAP similarity scores are available as Supporting Information. During pharmacophore generation, the FLAPpharm algorithm⁵⁶ in the FLAP package was used. The five selected compounds **7**, **19**, **23**, **24**, and **25** modeled generating a number of 30 conformers were automatically aligned by the software. The same procedure was used to align the five RdRP inhibitors used to validate the model.

Purities of the Acquired Compounds. Compounds **9–12** were purchased from Ambinter (www.ambinter.com, codes: Amb1938148, Amb10767907, Amb6474013, Amb1646026, respectively). Purity of the acquired compounds was determined by UHPLC on Agilent Technologies 6540 UHD Accurate Mass Q-TOF LC/MS, HPLC 1290 Infinity with DAD detector and evaluated to be higher than 95%. UHPLC conditions to assess the purity of acquired or final compounds were as follows: column, Phenomenex AERIS Peptide 1.2 mm × 1000 mm (1.7 μm); flow rate, 0.8 mL/min; acquisition time, 20 min; DAD 190–650 nm; oven temperature, 45 °C; gradient of acetonitrile in water containing 0.1% of formic acid (0–100% in 20 min).

Chemistry. Nuclear magnetic resonance (NMR) spectra were recorded on Bruker Advance II 400 MHz spectrometer at room temperature with tetramethylsilane and trichlorofluoromethane as internal standard. Chemical shifts (δ) are reported in parts per million (ppm), and peak multiplicity are reported as s (singlet), d (doublet), t (triplet), q (quartet), p (pentet), hept (heptet), m (multiplet), or br s (broad singlet). HRMS spectra were registered on Agilent Technologies 6540 UHD Accurate Mass Q-TOF LC/MS, HPLC 1290 Infinity. Purities of the final compounds were determined by UHPLC as described above for acquired compounds and were ≥98% pure. Methyl 5-(*p*-tolyl)-7-(trifluoromethyl)pyrazolo[1,5-*a*]pyrimidine-3-carboxylate, 5-(4-methoxyphenyl)-7-(trifluoromethyl)pyrazolo[1,5-*a*]pyrimidine-3-carboxylic acid, 5-phenyl-7-(trifluoromethyl)-[1,2,4]triazolo[1,5-*a*]pyrimidine-2-carboxylic acid were acquired from Specs and used without further purification. All other commercial products were acquired from Sigma-Aldrich; aniline and 2,5-dimethylaniline were freshly distilled before use.

5-(*p*-Tolyl)-7-(trifluoromethyl)pyrazolo[1,5-*a*]pyrimidine-3-carboxylic acid was obtained by ordinary hydrolysis of the corresponding methyl ester with potassium hydroxide in methanol.

2-(*sec*-Butylamino)- and 2-(phenylamino)benzoic acid **16a–b** were prepared by heating anthranilic anhydride (20.0 mmol) with *sec*-butylamine and aniline respectively, in DMF at 100 °C for 14 h.^{45,46} 3-Bromo-4-methylbenzoyl chloride was obtained by refluxing the corresponding acid in SOCl₂ for 4 h. After evaporation of the reagent excess at reduced pressure, the crude product was used without further purification. *N*-(3-Aminophenyl)benzamide was prepared by reacting benzoyl chloride with *tert*-butyl 3-aminophenylcarbamate followed by amino group deprotection upon heating at 140 °C. Tetrahydrofuran was distilled from sodium wire after the characteristic blue color of *in situ* generated sodium biphenyl ketyl (benzophenone-sodium “radical anion”) had been found to persist. Air- and moisture-sensitive compounds were stored in Schlenk tubes or Schlenk burets. They were handled under an atmosphere of 99.995% pure nitrogen, using appropriate glassware.

2-Amino-5,6-dihydro-4H-cyclopenta[*b*]thiophene-3-carboxamide (13a).⁴³ Cyclopentanone (8.57 g, 0.11 mol) and morpholine (9.74 g, 0.11 mol) were added dropwise to a stirred suspension of sulfur (3.27 g, 0.10 mol, 1.0 equiv) and cyanoacetamide (8.60 g, 0.10 mol) in ethanol (100 mL), and the mixture was stirred at 60 °C overnight. After cooling, the solid was filtered off, washed with MeOH,

and dried under a vacuum to afford a pale yellow solid (14% yield): mp 170–172 °C (lit.⁵⁹ mp 169–171 °C); ¹H NMR (DMSO-*d*₆) δ 7.15 (s, 2H), 6.47 (s, 2H), 2.78 (t, *J* = 7.2 Hz, 2H), 2.63 (t, *J* = 7.2 Hz, 2H), 2.26 (p, *J* = 7.1 Hz, 2H); ¹³C NMR (DMSO-*d*₆) δ 168.2, 166.1, 140.4, 119.8, 103.5, 30.4, 28.8, 27.6; HRMS: calcd for C₈H₁₀N₂OS 183.0592 (M + H⁺), found 183.0590 (M + H⁺).

2-Amino-4,5,6,7-tetrahydro-1-benzothiophene-3-carboxamide (13b).⁴³ The title compound was synthesized according to the procedure used for **13a** from cyclohexanone, to give a pale pink solid in 81% yield; mp 187–190 °C (lit.⁶⁰ mp 190 °C); ¹H NMR (CDCl₃) δ 6.16 (s, 2H), 5.52 (s, 2H), 2.69–2.60 (m, 2H), 2.59–2.42 (m, 2H), 1.92–1.68 (m, 4H); ¹³C NMR (CDCl₃) δ 168.4, 160.6, 129.0, 118.5, 107.4, 27.0, 24.4, 22.8 (2C); HRMS: calcd for C₉H₁₂N₂OS 197.0749 (M + H⁺), found 197.0749 (M + H⁺).

Ethyl 7-(difluoromethyl)-5-phenylpyrazolo[1,5-*a*]pyrimidine-3-carboxylate (14a).⁴⁴ A mixture of 4,4-difluoro-1-phenyl-1,3-butanedione (1.50 g, 7.6 mmol) and ethyl 3-amino-1H-pyrazole-4-carboxylate (1.17 g, 7.6 mmol) was refluxed in glacial acetic acid (3 mL) overnight. After cooling to room temperature, the resulting precipitate was filtered off, washed with water and dried. Trituration with petroleum ether gave a white solid (1.71 g, 71% yield) which was characterized as follows: mp 130–132 °C (lit.⁴⁴ mp 137 °C); ¹H NMR (CDCl₃) δ 8.60 (s, 1H), 8.34–8.19 (m, 2H), 7.74 (s, 1H), 7.63–7.54 (m, 3H), 7.40 (t, *J* = 5.3 Hz, 1H), 4.45 (q, *J* = 7.1 Hz, 2H), 1.47 (t, *J* = 7.2 Hz, 3H); ¹³C NMR (CDCl₃) δ 162.3, 159.2, 148.3, 148.0, 139.7 (t, *J* = 28 Hz), 135.8, 131.8, 129.2 (2C), 127.8 (2C), 108.0 (t, *J* = 24.2 Hz), 104.0, 103.3 (t, *J* = 4.9 Hz), 60.5, 14.5; ¹⁹F NMR (CDCl₃) δ –125.00 (d, *J* = 54 Hz, 2F); HRMS: calcd for C₁₆H₁₃F₂N₃O₂ 318.1054 (M + H⁺), found 318.1055 (M + H⁺).

Ethyl 7-(trifluoromethyl)-5-phenylpyrazolo[1,5-*a*]pyrimidine-3-carboxylate (14b).⁴⁴ The title compound was synthesized according to the procedure used for ester **14a**, but starting from 4,4,4-trifluoro-1-phenyl-1,3-butanedione instead of 4,4-difluoro-1-phenyl-1,3-butanedione, to give compound **14b** in 77% yield. Yellow solid, mp 110–112 °C (lit.⁴⁴ mp 111–113 °C); ¹H NMR (CDCl₃) δ 8.74 (s, 1H), 8.42–8.37 (m, 2H), 8.31 (s, 1H), 7.69–7.55 (m, 3H), 4.35 (q, *J* = 7.0 Hz, 2H), 1.38 (t, *J* = 7.0 Hz, 3H); ¹³C NMR (CDCl₃) δ 161.8, 158.8, 148.4, 148.3, 135.6, 134.3 (q, *J* = 37 Hz), 132.4, 129.6 (2C), 128.3 (2C), 119.2 (q, *J* = 27.5 Hz), 106.7 (q, *J* = 3.4 Hz), 103.7, 60.5, 14.4; ¹⁹F NMR (CDCl₃) δ –68.64 (3F); HRMS: calcd for C₁₆H₁₃F₃N₃O₂ 336.0960 (M + H⁺), found 336.0960 (M + H⁺).

7-(Difluoromethyl)-5-phenylpyrazolo[1,5-*a*]pyrimidine-3-carboxylic Acid (15a).⁴⁴ Ester **14a** (0.50 g, 1.6 mmol) was added to a KOH (0.50 g) dissolved in ethanol/water (10:1, 16.5 mL), and the resulting mixture was refluxed for 3 h. Upon cooling at room temperature, 5 N hydrochloric acid was added until complete precipitation of the product, which was filtered off and washed with water. After drying under a vacuum, a white solid in 78% yield was obtained; mp 225–230 °C; ¹H NMR (DMSO-*d*₆) δ 12.61 (s, 1H), 8.68 (s, 1H), 8.49–8.37 (m, 2H), 8.12 (s, 1H), 7.66 (t, *J* = 5.3 Hz, 1H), 7.66–7.56 (m, 3H); ¹³C NMR (DMSO-*d*₆) δ 168.2, 163.5, 152.5, 145.0 (t, *J* = 27 Hz), 140.8, 136.9 (2C), 134.3 (2C), 133.1, 133.0 (t, *J* = 9.9 Hz), 109.2 (t, *J* = 25.4 Hz), 109.1, 108.8; ¹⁹F NMR (DMSO-*d*₆) δ –67.50 (2F); HRMS: calcd for C₁₄H₉F₂N₃O₂ 290.0741 (M + H⁺), found 290.0744 (M + H⁺).

7-(Trifluoromethyl)-5-phenylpyrazolo[1,5-*a*]pyrimidine-3-carboxylic acid (15b).⁴⁴ The title compound was prepared following the same procedure as for acid **17a** but using ester **14b**. A white solid in 55% yield was obtained; mp 252–253 °C (lit.⁴⁴ mp 250–251 °C); ¹H NMR (DMSO-*d*₆) δ 12.65 (s, 1H), 8.74 (s, 1H), 8.45–8.39 (m, 2H), 8.35 (s, 1H), 7.68–7.53 (m, 3H); ¹³C NMR (DMSO-*d*₆) δ 163.3, 158.6, 148.9 (2C), 148.3 (2C), 135.7, 134.3 (q, *J* = 37 Hz), 132.4, 129.6, 128.4, 120.0 (q, *J* = 27.9 Hz), 106.7 (q, *J* = 3.3 Hz), 104.5; ¹⁹F NMR (DMSO-*d*₆) δ –67.50 (3F); HRMS: calcd for C₁₄H₈F₃N₃O₂ 308.0647 (M + H⁺), found 308.0649 (M + H⁺).

General Procedure To Prepare Amides 1–8. Oxalyl chloride (1.5 mmol) was added to a solution of the suitable carboxylic acid **15a–b** (1.0 mmol) and DMF (0.1 mmol) in dry DCM (3 mL), and the mixture was kept 2 h at 25 °C while stirring. After the solvent was evaporated at reduced pressure, the residue was dissolved in dry

dichloromethane (4 mL), the appropriate 2-amino-thiophene-3-carboxamide (1.0 mmol) and pyridine (2.0 mmol) were added, and the mixture was made to react at room temperature for 16 h. The solvent was evaporated at reduced pressure, and the residue was washed in sequence with diethyl ether (2×5 mL), 2 M sodium hydroxide, 2 M hydrochloric acid, and water. Finally, the residue was dried under a vacuum and chromatographed on silica gel (eluent, 9:1 dichloromethane/methanol mixture).

N-(3-Carbamoyl-5,6-dihydro-4H-cyclopenta[b]thiophen-2-yl)-7-(difluoromethyl)-5-phenylpyrazolo[1,5-a]pyrimidine-3-carboxamide (1). Yield, 69%. Yellow crystals, mp >270 °C; ^1H NMR (DMSO- d_6) δ 12.82 (s, 1H), 8.95–8.67 (m, 3H), 8.17 (s, 1H), 7.67 (t, J = 5.3 Hz, 1H), 7.87–7.42 (m, 3H), 7.54 (bs, 1H), 6.77 (s, 1H), 2.97 (t, J = 7.2 Hz, 2H), 2.84 (t, J = 7.4 Hz, 2H), 2.39 (p, J = 7.5 Hz, 2H); ^{13}C NMR (DMSO- d_6) δ 167.2, 159.6, 158.2, 148.3, 148.2, 145.8, 140.4 (t, J = 27 Hz), 139.6, 135.4, 132.8, 132.3, 129.6 (2C), 129.4 (2C), 112.3, 109.6 (t, J = 25.3 Hz), 105.2, 104.7 (t, J = 5.0 Hz), 29.7, 28.8, 28.2; ^{19}F NMR (DMSO- d_6) δ –124.47 (d, J = 52 Hz, 2F); HRMS: calcd for $\text{C}_{22}\text{H}_{17}\text{F}_3\text{N}_5\text{O}_2\text{S}$ 454.1149 ($\text{M} + \text{H}^+$), found 454.11496 ($\text{M} + \text{H}^+$).

N-(3-Carbamoyl-5,6-dihydro-4H-cyclopenta[b]thiophen-2-yl)-5-phenyl-7-(trifluoromethyl)pyrazolo[1,5-a]pyrimidine-3-carboxamide (2). Yield, 49%. Yellow crystals, mp >270 °C; ^1H NMR (DMSO- d_6) δ 12.84 (s, 1H), 9.00–8.78 (m, 3H), 8.38 (s, 1H), 7.96–7.40 (m, 4H), 6.79 (bs, 1H), 2.97 (t, J = 7.0 Hz, 2H), 2.83 (t, J = 7.1 Hz, 2H), 2.44–2.27 (m, 2H); ^{13}C NMR (DMSO- d_6) δ 167.4, 159.4, 158.0, 148.5, 148.3, 146.4, 139.0, 135.1, 134.6 (q, J = 37 Hz), 132.8, 132.5, 129.7 (2C), 129.6 (2C), 119.8 (q, J = 27.3 Hz), 112.6, 106.9, 105.7, 29.6, 28.2, 28.0; ^{19}F NMR (DMSO- d_6) δ –67.50 (3F); HRMS: calcd for $\text{C}_{22}\text{H}_{16}\text{F}_3\text{N}_5\text{O}_2\text{S}$ 472.1055 ($\text{M} + \text{H}^+$), found 472.1051 ($\text{M} + \text{H}^+$).

2-([5-Phenyl-7-(difluoromethyl)pyrazolo[1,5-a]pyrimidin-3-yl]-carbonylamino)-4,5,6,7-tetrahydrobenzo[b]thiophene-3-carboxamide (3). Yield, 59%. Yellow crystals, mp >270 °C; ^1H NMR (DMSO- d_6) δ 12.37 (s, 1H), 8.84–8.77 (m, 3H), 8.18 (s, 1H), 7.68 (t, J = 5.2 Hz, 1H), 7.74–7.58 (m, 3H), 7.54 (s, 1H), 7.04 (s, 1H), 3.02–2.70 (m, 2H), 2.70–2.61 (m, 2H), 1.94–1.64 (m, 4H); ^{13}C NMR (DMSO- d_6) δ 167.4, 159.5, 158.1, 148.2, 145.8, 142.0, 140.5 (t, J = 27 Hz), 135.4, 132.3, 129.7 (2C), 129.4 (2C), 129.3, 126.9, 117.6, 108.9 (t, J = 25.7 Hz), 105.3, 104.7 (t, J = 4.9 Hz), 25.6, 24.2, 23.0, 22.9; ^{19}F NMR (DMSO- d_6) δ –124.95 (d, J = 52 Hz, 2F); HRMS: calcd for $\text{C}_{23}\text{H}_{19}\text{F}_2\text{N}_5\text{O}_2\text{S}$ 468.1306 ($\text{M} + \text{H}^+$), found 468.1309 ($\text{M} + \text{H}^+$).

2-([5-Phenyl-7-(trifluoromethyl)pyrazolo[1,5-a]pyrimidin-3-yl]-carbonylamino)-4,5,6,7-tetrahydrobenzo[b]thiophene-3-carboxamide (4). Yield, 59%. Orange crystals, mp >270 °C; ^1H NMR (DMSO- d_6) δ 12.42 (s, 1H), 8.85 (s, 3H), 8.40 (s, 1H), 7.67 (m, 4H), 7.08 (bs, 1H), 2.78 (bs, 2H), 2.68 (bs, 2H), 1.77 (s, 4H); ^{13}C NMR (DMSO- d_6) δ 167.4, 159.4, 158.0, 148.5, 146.4, 142.0, 135.1, 134.6 (q, J = 37 Hz), 132.5, 129.7 (2C), 129.6 (2C), 129.4, 127.0, 119.8 (q, J = 27.3 Hz), 117.6, 106.9, 105.7, 25.7, 24.2, 23.0, 22.9; ^{19}F NMR (DMSO- d_6) δ –67.48 (s, 3F). HRMS: calcd for $\text{C}_{23}\text{H}_{18}\text{F}_3\text{N}_5\text{O}_2\text{S}$ 486.1206 ($\text{M} + \text{H}^+$), found 486.1215 ($\text{M} + \text{H}^+$).

2-([5-(p-Tolyl)-7-(trifluoromethyl)pyrazolo[1,5-a]pyrimidin-3-yl]-carbonylamino)-4,5,6,7-tetrahydrobenzo[b]thiophene-3-carboxamide (5). Yield, 47%. Yellow crystals, mp >270 °C; ^1H NMR (DMSO- d_6) δ 12.36 (s, 1H), 8.81 (s, 1H), 8.75 (d, J = 8.2 Hz, 2H), 8.36 (s, 1H), 7.59 (bs, 1H), 7.51 (d, J = 8.2 Hz, 2H), 7.07 (bs, 1H), 2.72 (bs, 2H), 2.67 (bs, 2H), 2.42 (s, 3H), 1.73 (bs, 4H); ^{13}C NMR (DMSO- d_6) δ 167.4, 159.3, 158.0, 148.4, 146.4, 142.9, 142.0, 134.5 (q, J = 38 Hz), 132.4, 130.3 (2C), 129.6 (2C), 129.3, 126.9, 119.8 (q, J = 27.5 Hz), 117.6, 106.7, 105.5, 25.6, 24.2, 23.1, 23.0, 21.6; ^{19}F NMR (DMSO- d_6) δ –67.46 (s, 3F). HRMS: calcd for $\text{C}_{24}\text{H}_{20}\text{F}_3\text{N}_5\text{O}_2\text{S}$ 500.1363 ($\text{M} + \text{H}^+$), found 500.1371 ($\text{M} + \text{H}^+$).

2-([5-(4-Methoxyphenyl)-7-(trifluoromethyl)pyrazolo[1,5-a]pyrimidin-3-yl]-carbonylamino)-4,5,6,7-tetrahydrobenzo[b]thiophene-3-carboxamide (6). Yield, 85%. Orange crystals, mp >270 °C; ^1H NMR (DMSO- d_6) δ 12.37 (s, 1H), 8.58 (d, J = 9.0 Hz, 2H), 8.79 (s, 1H), 8.32 (s, 1H), 7.62 (bs, 1H), 7.25 (d, J = 9.0 Hz, 2H), 7.07 (bs, 1H), 3.92 (s, 3H), 2.78 (bs, 2H), 2.68 (bs, 2H), 1.78 (bs, 4H); ^{13}C NMR (DMSO- d_6) δ 167.4, 163.3, 159.0, 158.0, 148.3, 146.4, 142.1, 134.3 (q, J = 37 Hz), 131.7 (2C), 129.3, 127.6, 126.9, 119.8 (q, J = 36.9 Hz), 117.5, 115.1 (2C), 106.4, 105.2, 56.1, 25.6, 24.2, 23.1, 23.0; ^{19}F

NMR (DMSO- d_6) δ –67.42 (s, 3F); HRMS: calcd for $\text{C}_{24}\text{H}_{20}\text{F}_3\text{N}_5\text{O}_2\text{S}$ 516.1312 ($\text{M} + \text{H}^+$), found 516.1318 ($\text{M} + \text{H}^+$).

2-([5-Phenyl-7-(trifluoromethyl)-[1,2,4]triazolo[1,5-a]pyrimidin-2-yl]-carbonylamino)-4,5,6,7-tetrahydrobenzo[b]thiophene-3-carboxamide (7). Yield, 75%. Yellow crystals, mp >270 °C; ^1H NMR (DMSO- d_6) δ 13.3 (s, 1H), 8.6 (s, 1H), 8.5–8.4 (m, 2H), 7.7 (m, 4H), 7.0 (s, 1H), 2.7 (dt, J = 32 and 6.0 Hz, 4H), 2.0–1.5 (m, 4H); ^{13}C NMR (DMSO- d_6) δ 167.7, 163.1, 158.9, 156.3, 155.1, 141.7, 135.3, 135.3 (q, J = 38 Hz), 133.1, 129.9, 129.8 (2C), 128.8 (2C), 128.0, 119.5 (q, J = 25.0 Hz), 118.0, 109.1, 25.7, 24.4, 22.9, 22.8; ^{19}F NMR (DMSO- d_6) δ –67.48 (s, 3F). HRMS: calcd for $\text{C}_{22}\text{H}_{17}\text{F}_3\text{N}_6\text{O}_2\text{S}$ 487.1164 ($\text{M} + \text{H}^+$), found 487.1161 ($\text{M} + \text{H}^+$).

2-(3-Pyridinecarbonylamino)-4,5,6,7-tetrahydrobenzo[b]thiophene-3-carboxamide (8). Yield, 71%. Yellow crystals, mp 233–235 °C; ^1H NMR (DMSO- d_6) δ 13.06 (s, 1H), 9.05 (s, 1H), 8.81 (d, J = 3.9 Hz, 1H), 8.22 (d, J = 8.0 Hz, 1H), 7.75 (bs, 1H), 7.63 (dd, J = 7.5 and 5.0 Hz, 1H), 7.15 (bs, 1H), 2.74 (bs, 2H), 2.66 (bs, 2H), 1.75 (bs, 4H); ^{13}C NMR (DMSO- d_6) δ 168.2, 161.5, 153.4, 148.6, 142.9, 135.4, 129.8, 128.7, 127.3, 124.6, 117.2, 25.6, 24.4, 22.9, 22.8; HRMS: calcd for $\text{C}_{15}\text{H}_{15}\text{N}_3\text{O}_2\text{S}$ 302.0963 ($\text{M} + \text{H}^+$), found 302.0965 ($\text{M} + \text{H}^+$).

2-(3-Bromobenzamido)-N-(sec-butyl)benzamide (17a). A mixture of 3-bromobenzoyl chloride (700 mg, 3.1 mmol), 2-amino-N-(sec-butyl)benzamide (16a) (600 mg, 3.1 mmol), and triethylamine (0.56 mL, 4.0 mmol) in toluene (40 mL) was kept at 110 °C for 14 h. After solvent evaporation at reduced pressure, the crude product was crystallized from methanol to obtain a white solid (81% yield) exhibiting the following properties: mp 133–134 °C; ^1H NMR (CDCl_3) δ 12.16 (s, 1H), 8.71 (d, J = 8.8 Hz, 1H), 8.19 (s, 1H), 7.90 (d, J = 8.3 Hz, 1H), 7.67 (d, J = 7.7 Hz, 1H), 7.59–7.45 (m, 2H), 7.38 (t, J = 7.9 Hz, 1H), 7.08 (t, J = 7.6 Hz, 1H), 6.30 (bd, J = 8.5 Hz, 1H), 4.13 (hept, J = 6.9 Hz, 1H), 1.61 (q, J = 7.2 Hz, 2H), 1.27 (d, J = 6.6 Hz, 3H), 0.99 (t, J = 7.4 Hz, 3H). ^{13}C NMR (CDCl_3) δ 168.6, 164.1, 139.4, 136.9, 134.8, 132.6, 131.1, 130.3, 126.6, 125.4, 123.2, 123.1, 121.6, 121.0, 47.3, 29.7, 20.4, 10.5; HRMS calcd for $\text{C}_{18}\text{H}_{19}\text{BrN}_2\text{O}_2$ 375.0703 ($\text{M} + \text{H}^+$), found 375.0715 ($\text{M} + \text{H}^+$).

2-(3-Bromo-4-methylbenzamido)-N-(sec-butyl)benzamide (17b). The title compound was prepared from 3-bromo-4-methylbenzoyl chloride and 2-amino-N-(sec-butyl)benzamide (16a), analogously to 17a, to give a white solid in 80% yield; mp 136–137 °C. ^1H NMR (CDCl_3) δ 12.07 (s, 1H), 8.72 (d, J = 8.2 Hz, 1H), 8.21 (d, J = 2.0 Hz, 1H), 7.81 (dd, J = 7.8 and 2.1 Hz, 1H), 7.57–7.29 (m, 3H), 7.08 (t, J = 6.5 and 5.5 Hz, 1H), 6.15 (bd, J = 9.5 Hz, 1H), 4.13 (hept, J = 7.0 Hz, 1H), 2.46 (d, J = 4.0 Hz, 3H), 1.60 (p, J = 7.3 Hz, 2H), 1.25 (d, J = 6.6 Hz, 3H), 0.98 (t, J = 7.4 Hz, 3H). ^{13}C NMR (CDCl_3) δ 168.6, 164.1, 142.0, 139.6, 134.2, 132.6, 132.0, 131.0, 126.4, 125.6, 125.4, 123.0, 121.6, 121.0, 47.3, 29.7, 23.1, 20.4, 10.5; HRMS calcd for $\text{C}_{19}\text{H}_{21}\text{BrN}_2\text{O}_2$ 389.0859 ($\text{M} + \text{H}^+$), found 389.0854 ($\text{M} + \text{H}^+$).

2-(3-Bromo-4-methylbenzamido)-N-(phenyl)benzamide (17c). The title compound was prepared according to the procedure used for 17b, from 3-bromo-4-methylbenzoyl chloride and 2-amino-N-(phenyl)benzamide (16b), to give a pale pink solid product in 88% yield; mp 215 °C (dec.). ^1H NMR (DMSO- d_6) δ 11.55 (s, 1H), 10.53 (s, 1H), 8.33 (d, J = 8.5 Hz, 1H), 8.08 (s, 1H), 7.90 (d, J = 7.9, 1H), 7.79 (d, J = 7.9 Hz, 1H), 7.72 (d, J = 8.5 Hz, 2H), 7.61 (t, J = 7.9 Hz, 1H), 7.55 (d, J = 7.8 Hz, 1H), 7.44–7.27 (m, 3H), 7.20–7.05 (m, 1H), 2.41 (s, 3H); ^{13}C NMR (DMSO- d_6) δ 167.7, 163.6, 142.1, 139.1, 138.6, 134.5, 132.5, 131.9, 131.4, 129.5, 129.1 (2C), 126.5, 124.9, 124.6, 124.4, 124.1, 122.3, 121.4 (2C), 23.0; HRMS: calcd for $\text{C}_{21}\text{H}_{17}\text{BrN}_2\text{O}_2$ 409.0546 ($\text{M} + \text{H}^+$), found 409.0550 ($\text{M} + \text{H}^+$).

General Procedure To Prepare Polyamido Products 10, 18–22.^{47,48} Butyllithium (20.3 mL, 1.48 M in hexanes, 30 mmol) was added dropwise at –75 °C to a solution of the appropriate bromo derivative (17a–c) (10 mmol) in tetrahydrofuran (100 mL), and the mixture was made to react for 10 min, under stirring, before the bath temperature was allowed to rise to –60 °C. Sulfur dioxide was bubbled into the mixture until its pH value reached 6–7. The cold bath was removed, and the temperature was allowed to rise to 25 °C. Hexane (20 mL) was added and the formed white precipitate was filtered, washed with hexane, and dried at 50 °C. The dry solid was suspended

in dichloromethane (20 mL), the mixture was cooled at 0 °C, and *N*-chlorosuccinimide (1.9 g, 14 mmol, 1.4 equiv) was added in portions. The mixture was made to react for 15 min at 0 °C, while stirring, and then it was kept at room temperature for further 25 min. The resulting suspension was filtered off on Celite, the solvent was evaporated at reduced pressure, and the solid residue was dissolved in acetone (20 mL). Triethylamine (1.4 mL, 10 mmol) and the suitable amine (10 mmol) were added, and the mixture was kept at room temperature for 12 h while stirring. After solvent evaporation at reduced pressure, chromatography of the residue on silica gel allowed collection of the pure product.

3-[2-(*sec*-Butylcarbamoyl)phenylcarbamoyl]-2-methyl-*N*-(2,5-dimethylphenyl)benzenesulfonamide (10). Yield, 19%. White rhombic crystals, mp 186–188 °C. ¹H NMR (DMSO-*d*₆) δ 12.61 (s, 1H), 9.71 (s, 1H), 8.70–8.39 (m, 2H), 8.27 (s, 1H), 8.01 (d, *J* = 7.5 Hz, 1H), 7.85–7.70 (m, 1H), 7.65 (d, *J* = 7.9 Hz, 1H), 7.55 (t, *J* = 7.9 Hz, 1H), 7.21 (t, *J* = 7.8 Hz, 1H), 6.95 (d, *J* = 7.7 Hz, 1H), 6.90 (d, *J* = 8.1 Hz, 1H), 6.75 (s, 1H), 3.97 (hept, *J* = 7.2 Hz, 1H), 2.58 (s, 3H), 2.12 (s, 3H), 1.98 (s, 3H), 1.61–1.53 (m, 2H), 1.13 (d, *J* = 6.2 Hz, 3H), 0.86 (t, *J* = 7.2 Hz, 3H); ¹³C NMR (DMSO-*d*₆) δ 168.3, 163.4, 142.1, 139.2, 135.9, 135.8, 134.7, 132.5, 131.5, 131.0, 130.6, 130.5, 130.2, 128.8, 127.8, 127.7, 126.2, 123.8, 121.8, 121.2, 47.0, 29.1, 23.1, 20.9, 20.4, 17.6, 11.1; HRMS: calcd for C₂₇H₃₁N₃O₄S 494.2114 (M + H⁺), found 494.2111 (M + H⁺).

3-[2-(*sec*-Butylcarbamoyl)phenylcarbamoyl]-*N*-(2,5-dimethylphenyl)benzene-sulfonamide (18). Yield, 18%. White rhombic crystals, mp 183–184 °C. ¹H NMR (DMSO-*d*₆) δ 12.61 (s, 1H), 9.67 (s, 1H), 8.70–8.39 (m, 2H), 8.25 (s, 1H), 8.11 (dt, *J* = 7.5 and 1.6 Hz, 1H), 7.89–7.73 (m, 3H), 7.56 (t, *J* = 7.9 Hz, 1H), 7.22 (t, *J* = 7.8 Hz, 1H), 6.99 (d, *J* = 7.7 Hz, 1H), 6.90 (d, *J* = 8.1 Hz, 1H), 6.76 (d, *J* = 2.3 Hz, 1H), 3.97 (hept, *J* = 7.4 Hz, 1H), 2.13 (s, 3H), 1.91 (s, 3H), 1.61–1.53 (m, 2H), 1.13 (d, *J* = 6.6 Hz, 3H), 0.85 (t, *J* = 7.5 Hz, 3H); ¹³C NMR (DMSO-*d*₆) δ 168.3, 163.4, 142.1, 139.2, 135.9, 135.8, 134.7, 132.5, 131.5, 131.0, 130.6, 130.5, 130.2, 128.8, 127.8, 127.7, 126.2, 123.8, 121.8, 121.2, 47.0, 29.1, 20.9, 20.4, 17.6, 11.1; HRMS: calcd for C₂₆H₂₉N₃O₄S 480.5986 (M + H⁺), found 480.1956 (M + H⁺).

3-[2-(*sec*-Butylcarbamoyl)phenylcarbamoyl]-*N*-phenylbenzenesulfonamide (19). Yield, 21%. White crystals, mp 207–208 °C. ¹H NMR (DMSO-*d*₆) δ 12.64 (s, 1H), 10.46 (s, 1H), 8.62–8.48 (m, 2H), 8.35 (t, *J* = 1.8 Hz, 1H), 8.08 (d, *J* = 8.0 Hz, 1H), 8.00–7.90 (m, 1H), 7.85 (dd, *J* = 7.9 and 1.5 Hz, 1H), 7.77 (t, *J* = 7.8 Hz, 1H), 7.56 (ddd, *J* = 8.6, 7.4, and 1.5 Hz, 1H), 7.26–7.16 (m, 3H), 7.16–7.07 (m, 2H), 7.01 (tt, *J* = 7.1 and 1.2 Hz, 1H), 3.97 (hept, *J* = 6.8 Hz, 1H), 1.60–1.45 (m, 2H), 1.13 (d, *J* = 6.6 Hz, 3H), 0.85 (t, *J* = 7.4 Hz, 3H); ¹³C NMR (DMSO-*d*₆) δ 168.3, 163.2, 140.9, 139.2, 137.8, 135.9, 132.5, 131.0, 130.7, 130.3, 129.7 (2C), 128.8, 126.3, 124.8, 123.8, 121.7, 121.1, 120.7 (2C), 47.1, 29.1, 20.4, 11.2; HRMS: calcd for C₂₄H₂₅N₃O₄S 452.5454 (M + H⁺), found 452.1651 (M + H⁺).

5-[2-(*sec*-Butylcarbamoyl)phenylcarbamoyl]-2-methyl-*N*-[(3-benzamido)-phenyl]benzenesulfonamide (20). Yield, 22%. White crystalline, mp 155–157 °C. ¹H NMR (DMSO-*d*₆) δ 12.57 (s, 1H), 10.63 (s, 1H), 10.20 (s, 1H), 8.66–8.48 (m, 3H), 7.97 (dd, *J* = 7.9 and 1.9 Hz, 1H), 7.89–7.80 (m, 3H), 7.69 (t, *J* = 2.0 Hz, 1H), 7.66–7.50 (m, 3H), 7.47–7.40 (m, 2H), 7.40–7.35 (m, 1H), 7.26–7.13 (m, 2H), 6.87 (ddd, *J* = 8.2, 2.1, and 1.0 Hz, 1H), 3.96 (hept, *J* = 7.2 Hz, 1H), 2.68 (s, 3H), 1.62–1.41 (m, 2H), 1.12 (d, *J* = 6.6 Hz, 3H), 0.85 (t, *J* = 7.4 Hz, 3H). ¹³C NMR (DMSO-*d*₆) δ 168.4, 166.0, 163.5, 141.3, 140.4, 139.4, 138.8, 138.1, 135.2, 133.8, 133.2, 132.5, 132.0, 131.1, 129.7, 129.4, 128.8, 128.7 (2C), 128.1 (2C), 123.5, 121.7, 121.0, 116.1, 114.6, 111.5, 47.1, 29.1, 20.4, 20.3, 11.1; HRMS: calcd for C₃₂H₃₂N₄O₅S 585.6927 (M + H⁺), found 585.2173 (M + H⁺).

3-(*N*-(2,5-Dimethylphenyl)sulfamoyl)-4-methyl-*N*-(2-(phenylcarbamoyl)phenyl)benzamide (21). Yield, 24%. White rhombic crystals, mp 235 °C (dec.). ¹H NMR (DMSO-*d*₆) δ 11.70 (s, 1H), 10.53 (s, 1H), 9.70 (s, 1H), 8.35 (dd, *J* = 8.3 and 1.3 Hz, 1H), 8.29 (d, *J* = 1.9 Hz, 1H), 8.01 (dd, *J* = 8.0 and 2.0 Hz, 1H), 7.94–7.88 (m, 1H), 7.72 (d, *J* = 7.6 Hz, 2H), 7.61 (dd, *J* = 7.8 and 6.0 Hz, 2H), 7.36 (t, *J* = 7.9 Hz, 2H), 7.31 (t, *J* = 7.5 Hz, 1H), 7.14 (t, *J* = 7.3 Hz, 1H), 7.00 (d, *J* = 7.7 Hz, 1H), 6.89 (d, *J* = 7.9 Hz, 1H), 6.75 (s, 1H),

2.57 (s, 3H), 2.09 (s, 3H), 1.97 (s, 3H); ¹³C NMR (DMSO-*d*₆) δ 167.7, 163.6, 141.4, 140.3, 139.0, 138.6, 136.0, 134.6, 133.7, 132.8, 132.6, 131.8, 131.0, 130.8, 129.4, 129.1 (2C), 128.6, 128.0, 127.9, 124.7, 124.1, 124.0, 122.2, 121.5 (2C), 20.8, 20.6, 17.6; HRMS: calcd for C₂₉H₂₇N₃O₄S 514.1801 (M + H⁺), found 514.1797 (M + H⁺).

3-[2-(*sec*-Butylcarbamoyl)phenylcarbamoyl]-*N*-(4-hydroxyphenyl)benzenesulfonamide (22). Yield, 26%. White solid, mp 202 °C (dec.). ¹H NMR (DMSO-*d*₆) δ 12.61 (s, 1H), 9.88 (s, 1H), 9.28 (s, 1H), 8.59–8.49 (m, 2H), 8.28 (s, 1H), 8.07 (d, *J* = 8.0 Hz, 1H), 7.89–7.70 (m, 3H), 7.56 (t, *J* = 7.6 Hz, 1H), 7.22 (t, *J* = 7.6 Hz, 1H), 6.85 (d, *J* = 8.7 Hz, 2H), 6.59 (d, *J* = 8.7 Hz, 2H), 3.98 (hept, *J* = 6.5 Hz, 1H), 1.59–1.44 (m, 2H), 1.14 (d, *J* = 6.7 Hz, 3H), 0.86 (t, *J* = 7.4 Hz, 3H). ¹³C NMR (DMSO-*d*₆) δ 167.8, 162.9, 155.0, 140.5, 138.8, 135.3, 132.1, 130.1, 130.0, 129.9, 128.3, 128.0, 125.9, 124.3 (2C), 123.2, 121.2, 120.6, 115.6 (2C), 46.6, 28.6, 19.9, 10.7; HRMS: calcd for C₂₄H₂₅N₃O₅S 468.5986 (M + H⁺), found 468.1599 (M + H⁺).

Biology. Compounds and Peptide. Each test compound was dissolved in DMSO 100%. RBV (1-D-ribofuranosyl-1,2,4-triazole-3-carboxamide) was obtained from Roche. The PB1_(1–15)-Tat peptide was synthesized and purified by the Peptide Facility of CRIBI Biotechnology Center (University of Padua, Padua, Italy). This peptide contains the first 15 N-terminal amino acids of PB1 protein conjugated to the C-terminal sequence of HIV Tat protein (amino acids 47–59), which allows intracellular delivery.

Plasmids. Plasmids pcDNA-PB1, pcDNA-PB2, pcDNA-PA, and pcDNA-NP, containing cDNA copies of the influenza A/PR/8/34 virus PB1, PB2, PA, and NP genes, respectively, were created as described elsewhere⁴⁹ and kindly provided by P. Digard (Roslin Institute, University of Edinburgh, United Kingdom). Plasmid pPoll-Flu-*fluc*, which contains an influenza virus-based luciferase minireplicon vRNA under the control of the human RNA polymerase I promoter, was provided by L. Tiley (University of Cambridge, United Kingdom). Plasmid pRL-SV40 expressing the *Renilla* luciferase was purchased from Promega.

Cells and Virus. Mardin-Darby canine kidney (MDCK) and human embryonic kidney (HEK) 293T cells were cultured in Dulbecco's modified Eagle's medium (DMEM, Life Technologies) supplemented with 10% (v/v) fetal bovine serum (FBS, Life Technologies) and antibiotics (100 U/mL penicillin and 100 µg/mL streptomycin, Life Technologies) at 37 °C in a humidified atmosphere with 5% CO₂. Influenza A/PR/8/34 virus (H1N1, Cambridge lineage) was obtained from P. Digard (Roslin Institute, University of Edinburgh, United Kingdom). The FluA viruses A/Wisconsin/67/05 and A/Solomon Island/3/06, and the influenza B/Malaysia/2506/4 virus were provided by R. Cusinato (Clinical Microbiology and Virology Unit, Padua University Hospital, Padua, Italy). Influenza B/Lee/40 virus was obtained from W. S. Barclay (Imperial College, London, United Kingdom). The clinical isolate A/Parma/24/09 was kindly provided by I. Donatelli (Istituto Superiore di Sanità, Rome, Italy); the local strain A/Padova/30/2011 of the pandemic FluA H1N1 virus was donated by C. Salata and A. Calistri (University of Padua, Padua, Italy). All influenza viruses were propagated in MDCK cells.

Protein Expression and Purification. *Escherichia coli*-expressed, purified GST and GST-PB1_(1–25) proteins were obtained as previously described.^{13,61,62} The 6His-PA_(239–716) protein was expressed in *E. coli* strain BL21(DE3)pLysS and purified as described.^{13,16}

PA–PB1 Interaction Enzyme-Linked Immunosorbent Assay (ELISA). To analyze the ability of each test compound to dissociate the PA–PB1 interaction *in vitro*, a procedure already described¹³ was followed. Briefly, microtiter plates (Nuova Aptca) were coated with 400 ng of purified 6His-PA_(239–716) for 3 h at 37 °C and then blocked with 2% BSA (Sigma) in PBS for 1 h at 37 °C. After washing with PBS plus 0.3% Tween 20, 200 ng of GST-PB1_(1–25), or of GST alone as a control, in the absence or the presence of test compounds at various concentrations (10, 50, 100, 200 µM) were added and incubated O/N at room temperature. After washing, the interaction between 6His-PA_(239–716) and GST-PB1_(1–25) was detected by an anti-GST monoclonal antibody conjugated to horseradish peroxidase (HRP) (GenScript; diluted 1:3000 in PBS plus 2% FBS). Following washes

with PBS plus 0.3% Tween 20, the chromogenic substrate 3,3',5,5'-tetramethylbenzidine (TMB, KPL) was added, and the consequent color development was measured at 450 nm by an ELISA plate reader (Tecan Sunrise). Values obtained from the samples treated with only DMSO were used to set as 100% of PA–PB1 interaction.

Cytotoxicity Assays. Cytotoxicity of compounds was tested in MDCK and HEK 293T cells by the 3-(4,5-dimethylthiazol-2-yl)-2,5-diphenyl tetrazolium bromide (MTT) method, as previously reported.¹² Briefly, HEK 293T or MDCK cells (2×10^4 per well) were cultured in 96-well plates at 37 °C for 24 or 48 h, respectively, in DMEM containing serially diluted compounds (from 250 to 1.9 μ M). Then, MTT solution (5 mg/mL in PBS) was added to each well and plates were incubated for 4 h at 37 °C. Successively, a solubilization solution was added to lyse cells. After 3 h of further incubation at 37 °C, absorbance was read at 620 nm using an ELISA plate reader (Tecan Sunrise).

Plaque Reduction Assays (PRA). The experiments were carried out as previously described.¹³ Briefly, in a 12-well plates format, a confluent monolayer of MDCK cells were infected with all FluA or FluB virus assessed at approximately 40 PFU/well in DMEM supplemented with 1 μ g/mL of TPCK-treated trypsin (Worthington Biochemical Corporation) and 0.14% BSA and incubated for 1 h at 37 °C. The influenza viruses infection was performed in the presence of different concentrations of test compounds or solvent (DMSO) as a control. Serum-free medium containing 1 μ g/mL of TPCK-treated trypsin, 0.14% BSA, 1.2% Avicel, and DMSO or test compounds at the indicated concentrations was added after 1 h of virus adsorption. After 48 h of incubation, cells were fixed with 4% formaldehyde and stained with 0.1% toluidine blue. Viral plaques were counted, and the mean plaque number in the DMSO-treated control was set at 100%.

Minireplicon Assays. HEK 293T cells were seeded at 10^5 per well on 24-well plates. After 24 h, cells were transiently transfected, in the presence of the test compounds at different concentrations or DMSO, with pcDNA-PB1, pcDNA-PB2, pcDNA-PA, pcDNA-NP plasmids (100 ng/well of each) along with pPoll-Flu- β Luc plasmid (50 ng/well) as described elsewhere.¹³ In addition, a plasmid constitutively expressing *Renilla* luciferase, pRL-SV40 (50 ng/well), was included in the transfection mixture to normalize variations in transfection efficiency. After 4 h, the medium was replaced with fresh DMEM containing DMSO or test compounds. At 24 h post-transfection, cells were lysed, and the relative firefly and *Renilla* luciferase activities were determined using the Dual Luciferase Assay Kit from Promega and a luminescence counter (Victor X2, PerkinElmer). The luciferase activities of the samples treated with DMSO (no test compound) were set as 100%.

UL54–UL44 Interaction ELISA. This assay was conducted as previously described,⁵³ with minor modifications. Briefly, microtiter plates were coated with 0.2 mg of purified baculovirus-expressed HCMV UL54 and blocked with 2% BSA (Sigma) in PBS for 1 h. After washing, 0.5 mg of purified baculovirus-expressed UL44, mixed with each compound at different concentrations or with DMSO alone at a final 1% concentration (no compound), was added and incubated for 1 h at 37 °C. Following further washes, the wells were incubated with monoclonal antibody (mAb) YL1/2, which recognizes the EEF epitope inserted at the C terminus of UL44,⁵² for 1 h at 37 °C. Plates were then washed and incubated with horseradish peroxidase (HRP)-conjugated anti-rat antibody (Sigma). Following washes with PBS plus 0.3% Tween 20, the chromogenic substrate 3,3',5,5'-tetramethylbenzidine (TMB) (KPL) was added, and absorbance was read at 450 nm on an ELISA plate reader (Tecan Sunrise).

■ ASSOCIATED CONTENT

■ Supporting Information

Table containing structures of the 293 compounds used for ligand-based virtual screening and their FLAP similarity score. Validation of the pharmacophore using literature data. Methods for preliminary ADME assays. Figure reporting data of compounds activity in the UL54–UL44 interaction ELISA.

This material is available free of charge via the Internet at <http://pubs.acs.org>.

■ AUTHOR INFORMATION

Corresponding Authors

*(L.G.) Phone, +39 075 585 5632; fax, +39 075 45646; e-mail, laura.goracci@unipg.it.

*(A.L.) Phone, +39 049 8272363; fax, +39 049 8272355; e-mail, arianna.loregian@unipd.it.

Author Contributions

[#]S.L. and G.N. contributed equally to this work.

Author Contributions

^{||}L.G. and A.L. contributed equally to this work.

Notes

The authors declare no competing financial interest.

■ ACKNOWLEDGMENTS

We thank P. Digard, R. Cusinato, A. Calistri, C. Salata, I. Donatelli, and W. S. Barclay for FluA and FluB viruses; P. Digard and L. Tiley for plasmids; A. Valeri for collaboration in metabolic stability assay; and R. Alvarez and S. Wendelspiess at F. Hoffmann-La Roche Ltd. for permeability assays. We also thank P. Digard for helpful suggestions. This work was supported by Italian Ministry of Health and Istituto Superiore Sanità, Progetto Finalizzato 2009 “Studio e Sviluppo di Nuovi Farmaci Antivirali Contro Infezioni da Virus Influenzale A-H1N1” (to V.C., A.L., G.P., and O.T.) and by ESCMID Research Grant 2013 (to B.M.).

■ ABBREVIATIONS

NA, neuraminidase; CC₅₀, concentration that causes a decrease of cell viability of 50%; Flu, influenza virus; FluA, influenza A virus; FluB, influenza B virus; HEK, human embryonic kidney; HLM, human liver microsomes; PAMPA, parallel artificial membrane permeability assay; MDCK, Mardin–Darby canine kidney; NP, nucleoprotein; PA, polymerase acidic protein; PB1, polymerase basic protein 1; PB2, polymerase basic protein 2; PRA, plaque reduction assays; RBV, ribavirin; RdRP, RNA-dependent RNA polymerase; RNP, ribonucleoprotein; SAR, structure–activity relationship; ADME, absorption, distribution, metabolism and excretion; HCMV, human cytomegalovirus

■ REFERENCES

- (1) Harper, S. A.; Bradley, J. S.; Englund, J. A.; File, T. M.; Gravenstein, S.; Hayden, F. G.; McGeer, A. J.; Neuzil, K. M.; Pavia, A. T.; Tapper, M. L.; Uyeki, T. M.; Zimmerman, R. K. Seasonal influenza in adults and children—diagnosis, treatment, chemoprophylaxis, and institutional outbreak management: clinical practice guidelines of the Infectious Diseases Society of America. *Clin. Infect. Dis.* **2009**, *48*, 1003–1032.
- (2) Das, K. Antivirals targeting influenza A virus. *J. Med. Chem.* **2012**, *55*, 6263–6277.
- (3) Hurt, A. C.; Chotpitayasunondh, T.; Cox, N. J.; Daniels, R.; Fry, A. M.; Gubareva, L. V.; Hayden, F. G.; Hui, D. S.; Hungnes, O.; Lackenby, A.; Lim, W.; Meijer, A.; Penn, C.; Tashiro, M.; Uyeki, T. M.; Zambon, M. Antiviral resistance during the 2009 influenza A H1N1 pandemic: public health, laboratory, and clinical perspectives. *Lancet Infect. Dis.* **2012**, *12*, 240–248.
- (4) Moss, R. B.; Davey, R. T.; Steigbigel, R. T.; Fang, F. Targeting pandemic influenza: a primer on influenza antivirals and drug resistance. *J. Antimicrob. Chemother.* **2010**, *65*, 1086–1093.

- (5) Colman, P. M.; Varghese, J. N.; Laver, W. G. Structure of the catalytic and antigenic sites in influenza virus neuraminidase. *Nature* **1983**, *303*, 41–44.
- (6) Jackson, R. J.; Cooper, K. L.; Tappenden, P.; Rees, A.; Simpson, E. L.; Read, R. C.; Nicholson, K. G. Oseltamivir, zanamivir and amantadine in the prevention of influenza: a systematic review. *J. Infect.* **2011**, *62*, 14–25.
- (7) von Itzstein, M.; Wu, W. Y.; Kok, G. B.; Pegg, M. S.; Dyason, J. C.; Jin, B.; Van Phan, T.; Smythe, M. L.; White, H. F.; Oliver, S. W.; Colman, P. M.; Varghese, J. N.; Ryan, D. M.; Woods, J. M.; Bethell, R.; Hotham, V. J.; Cameron, J. M.; Penn, C. R. Rational design of potent sialidase-based inhibitors of influenza virus replication. *Nature* **1993**, *363*, 418–423.
- (8) Goodford, P. J. A computational procedure for determining energetically favorable binding sites on biologically important macromolecules. *J. Med. Chem.* **1985**, *28*, 849–857.
- (9) Samson, M.; Pizzorno, A.; Abed, Y.; Boivin, G. Influenza virus resistance to neuraminidase inhibitors. *Antiviral Res.* **2013**, *98*, 174–185.
- (10) Loregian, A.; Mercorelli, B.; Nannetti, G.; Compagnin G.; Palù, G. Antiviral strategies against influenza virus: towards new therapeutic approaches. *Cell. Mol. Life Sci.* **2014**, [Online early access]. DOI 10.1007/s00018-014-1615-2.
- (11) Suzuki, T.; Aina, A.; Nagata, N.; Sata, T.; Sawa, H.; Hasegawa, H. A novel function of the N-terminal domain of PA in assembly of influenza A virus RNA polymerase. *Biochem. Biophys. Res. Commun.* **2011**, *414*, 719–726.
- (12) Yamada, K.; Koyama, H.; Hagiwara, K.; Ueda, A.; Sasaki, Y.; Kanesashi, S. N.; Ueno, R.; Nakamura, H. K.; Kuwata, K.; Shimizu, K.; Suzuki, M.; Aida, Y. Identification of a novel compound with antiviral activity against influenza A virus depending on PA subunit of viral RNA polymerase. *Microbes Infect.* **2012**, *14*, 740–747.
- (13) Muratore, G.; Goracci, L.; Mercorelli, B.; Foeglein, Á.; Digard, P.; Cruciani, G.; Palù, G.; Loregian, A. Small molecule inhibitors of influenza A and B viruses that act by disrupting subunit interactions of the viral polymerase. *Proc. Natl. Acad. Sci. U.S.A.* **2012**, *109*, 6247–6252.
- (14) Muratore, G.; Mercorelli, B.; Goracci, L.; Cruciani, G.; Digard, P.; Palù, G.; Loregian, A. The human cytomegalovirus inhibitor AL18 also possesses activity against influenza A and B viruses. *Antimicrob. Agents Chemother.* **2012**, *56*, 6009–6013.
- (15) Kessler, U.; Castagnolo, D.; Pagano, M.; Deodato, D.; Bernardini, M.; Pilger, B.; Ranadheera, C.; Botta, M. Discovery and synthesis of novel benzofuran derivatives as inhibitors of influenza A virus. *Med. Chem. Lett.* **2013**, *23*, 5575–5577.
- (16) Massari, S.; Nannetti, G.; Goracci, L.; Sancineto, L.; Muratore, G.; Sabatini, S.; Manfroni, G.; Mercorelli, B.; Cecchetti, V.; Facchini, M.; Palù, G.; Cruciani, G.; Loregian, A.; Tabarrini, O. Structural investigation of cycloheptathiophene-3-carboxamide derivatives targeting influenza virus polymerase assembly. *J. Med. Chem.* **2013**, *56*, 10118–10131.
- (17) Pagano, M.; Castagnolo, D.; Bernardini, M.; Fallacara, A. L.; Laurenzana, I.; Deodato, D.; Kessler, U.; Pilger, B.; Stergiou, L.; Strunze, S.; Tintori, C.; Botta, M. The Fight against the influenza A virus H1N1: synthesis, molecular modeling, and biological evaluation of benzofuran derivatives as viral RNA polymerase inhibitors. *Chem. Med. Chem.* **2014**, *9*, 129–150.
- (18) Tintori, C.; Laurenzana, I.; Fallacara, A. L.; Kessler, U.; Pilger, B.; Stergiou, L.; Botta, M. High-throughput docking for the identification of new influenza A virus polymerase inhibitors targeting the PA-PB1 protein-protein interaction. *Bioorg. Med. Chem. Lett.* **2014**, *24*, 280–282.
- (19) Palese, P.; Shaw, M. L. Orthomyxoviridae: The viruses and their replication. In *Fields Virology*, 5th ed.; Knipe, D. M.; Howley, P. M., Eds.; Lippincott Williams and Wilkins: Philadelphia, PA, 2007; Vol. 2, pp 1647–1689.
- (20) Horisberger, M. A. The large P proteins of influenza A viruses are composed of one acidic and two basic polypeptides. *Virology* **1980**, *107*, 302–305.
- (21) Nagata, K.; Kawaguchi, A.; Naito, T. Host factors for replication and transcription of the influenza virus genome. *Rev. Med. Virol.* **2008**, *18*, 247–260.
- (22) Palù, G.; Loregian, A. Inhibition of herpesvirus and influenza virus replication by blocking polymerase subunit interactions. *Antiviral Res.* **2013**, *99*, 318–327.
- (23) Obayashi, E.; Yoshida, H.; Kawai, F.; Shibayama, N.; Kawaguchi, A.; Nagata, K.; Tame, J. R.; Park, S. Y. The structural basis for an essential subunit interaction in influenza virus RNA polymerase. *Nature* **2008**, *454*, 1127–1131.
- (24) He, X.; Zhou, J.; Bartlam, M.; Zhang, R.; Ma, J.; Lou, Z.; Li, X.; Li, J.; Joachimiak, A.; Zeng, Z.; Ge, R.; Rao, Z.; Liu, Y. Crystal structure of the polymerase PA_C-PB1_N complex from an avian influenza H5N1 virus. *Nature* **2008**, *454*, 1123–1126.
- (25) Sugiyama, K.; Obayashi, E.; Kawaguchi, A.; Suzuki, Y.; Tame, J. R.; Nagata, K.; Park, S. Y. Structural insight into the essential PB1–PB2 subunit contact of the influenza virus RNA polymerase. *EMBO J.* **2009**, *28*, 1803–1811.
- (26) Reuther, P.; Mänz, B.; Brunotte, L.; Schwemmle, M.; Wunderlich, K. Targeting of the influenza A virus polymerase PB1–PB2 interface indicates strain-specific assembly differences. *J. Virol.* **2011**, *85*, 13298–13309.
- (27) Kessler, U.; Mayer, D.; Wunderlich, K.; Ranadheera, C.; Schwemmle, M. Influenza A and B virus replication-inhibiting peptides. U.S. Patent 0129764, May 24, 2012.
- (28) Ghanem, A.; Mayer, D.; Chase, G.; Tegge, W.; Frank, R.; Kochs, G.; García-Sastre, A.; Schwemmle, M. Peptide-mediated interference with influenza A virus polymerase. *J. Virol.* **2007**, *81*, 7801–7804.
- (29) Scognamiglio, P. L.; Di Natale, C.; Perretta, G.; Marasco, D. From peptides to small molecules: an intriguing but intricate way to new drugs. *Curr. Med. Chem.* **2013**, *20*, 3803–3817.
- (30) Hagmann, W. K. The many roles for fluorine in medicinal chemistry. *J. Med. Chem.* **2008**, *51*, 4359–4369.
- (31) Filler, R.; Saha, R. Fluorine in medicinal chemistry: a century of progress and a 60-year retrospective of selected highlights. *Future Med. Chem.* **2009**, *1*, 777–791.
- (32) Purser, S.; Moore, P. R.; Swallow, S.; Gouverneur, V. Fluorine in medicinal chemistry. *Chem. Soc. Rev.* **2008**, *37*, 320–330.
- (33) Kobayashi, Y.; Taguchi, T. Fluorine-modified vitamin D₃ analogs. *J. Synth. Org. Chem. Jpn.* **1985**, *43*, 1073–1082.
- (34) Tandon, M.; O'Donnell, M. M.; Porte, A.; Vensel, D.; Yang, D.; Palma, R.; Beresford, A.; Ashwell, M. A. The design and preparation of metabolically protected new arylpiperazine 5-HT_{1A} ligands. *Bioorg. Med. Chem. Lett.* **2004**, *14*, 1709–1712.
- (35) Böhm, H. J.; Banner, D.; Bendels, S.; Kansy, M.; Kuhn, B.; Müller, K.; Obst-Sander, U.; Stahl, M. Fluorine in medicinal chemistry. *ChemBioChem* **2004**, *5*, 637–643.
- (36) Smart, B. E. Fluorine substituent effects (on bioactivity). *J. Fluorine Chem.* **2001**, *109*, 3–11.
- (37) Van Niel, M. B.; Beer, M. S.; Broughton, H. B.; Cheng, S. K.; Goodacre, S. C.; Heald, A.; XLocker, K. L.; MacLeod, A. M.; Morrison, D.; Moyes, C. R.; O'Connor, D.; Pike, A.; Rowley, M.; Russel, M. G.; Sohal, B.; Stanton, J. A.; Thomas, S.; Verrier, H.; Watt, A. P.; Castro, J. L. Fluorination of 3-(3-(piperidin-1-yl)propyl)indoles and 3-(3-(piperazin-1-yl)propyl)indoles gives selective human 5-HT_{1D} receptor ligands with improved pharmacokinetic profiles. *J. Med. Chem.* **1999**, *42*, 2087–2104.
- (38) Okamoto, S.; Tanaka, Y.; DeLuca, H. F.; Kobayashi, Y.; Ikekawa, N. Biological activity of 24,24-difluoro-1,25-dihydroxyvitamin D₃. *Am. J. Physiol.* **1983**, *244*, E159–163.
- (39) Abbate, F.; Casini, A.; Scozzafava, A.; Supuran, C. T. Carbonic anhydrase inhibitors: X-ray crystallographic structure of the adduct of human isozyme II with the perfluorobenzoyl analogue of methazolamide. Implications for the drug design of fluorinated inhibitors. *J. Enzyme Inhib. Med. Chem.* **2003**, *18*, 303–308.
- (40) Zhang, W.; Wang, F.; Hu, J. N-tosyl-S-difluoromethyl-S-phenylsulfoximine: a new difluoromethylation reagent for S-, N-, and C-nucleophiles. *Org. Lett.* **2009**, *11*, 2109–2112.

- (41) Baroni, M.; Cruciani, G.; Sciabola, S.; Perruccio, F.; Mason, J. S. A common reference framework for analyzing/comparing proteins and ligands. Fingerprints for Ligands And Proteins (FLAP): theory and application. *J. Chem. Inf. Model* **2007**, *47*, 279–294.
- (42) Goodford, P. J. The Basic Principles of GRID. In *Molecular Interaction Fields: Applications in Drug Discovery and ADME Prediction*; Cruciani, G., Ed.; Wiley-VCH: Weinheim, Germany, 2006; pp 1–25.
- (43) Gewalt, K.; Schinke, E.; Böttcher, H. Heterocyclen aus CH-aciden Nitrilen, VIII. 2-amino-thiophene aus methylenaktiven nitrilen, carbonylverbindungen und schwefel. *Chem. Ber.* **1966**, *99*, 94–100.
- (44) Yoshida, M.; Mori, A.; Inaba, A.; Oka, M.; Makino, H.; Yamaguchi, M.; Fujita, H.; Kawamoto, T.; Goto, M.; Kimura, H.; Baba, A.; Yasuma, T. Synthesis and structure-activity relationship of tetrahydropyrazolopyrimidine derivatives-A novel structural class of potent calcium-sensing receptor antagonists. *Bioorg. Med. Chem.* **2010**, *18*, 8501–8511.
- (45) Asano, T.; Yoshikawa, T.; Usui, T.; Yamamoto, H.; Yamamoto, Y.; Uehara, Y.; Nakamura, H. Benzamides and benzamidines as specific inhibitors of epidermal growth factor receptor and v-Src protein tyrosine kinases. *Bioorg. Med. Chem.* **2004**, *12*, 3529–3542.
- (46) Bunnett, J. F.; Naff, M. B. Kinetics of reactions of amines with isatoic anhydride. *J. Am. Chem. Soc.* **1966**, *88*, 4001–4008.
- (47) Graham, S. L.; Hoffman, J. M.; Gautheron, P.; Michelson, S. R.; Scholz, T. H.; Schwam, H.; Shepard, K. L.; Smith, A. M.; Smith, R. L.; Sondey, J. M.; Sugrue, M. F. Topically active carbonic anhydrase inhibitors. 3. Benzofuran- and indole-2-sulfonamides. *J. Med. Chem.* **1990**, *33*, 749–754.
- (48) Graham, S. L.; Scholz, T. H. The reaction of sulfinic acid salts with hydroxylamine-O-sulfonic acid. A useful synthesis of primary sulfonamides. *Synthesis* **1986**, *12*, 1031–1032.
- (49) Mullin, A. E.; Dalton, R. M.; Amorim, M. J.; Elton, D.; Digard, P. Increased amounts of the influenza virus nucleoprotein do not promote higher levels of viral genome replication. *J. Gen. Virol.* **2004**, *85*, 3689–3698.
- (50) Sidwell, R. W.; Huffman, J. H.; Khare, G. P.; Allen, L. B.; Witkowski, J. T.; Robins, R. K. Broad-spectrum antiviral activity of Virazole: 1-Beta-Dribofuranosyl-1,2,4-triazole-3-carboxamide. *Science* **1972**, *177*, 705–706.
- (51) Liu, H.; Yao, X. Molecular basis of the interaction for an essential subunit PA-PB1 in influenza virus RNA polymerase: Insights from molecular dynamics simulation and free energy calculation. *Mol. Pharmaceutics* **2010**, *7*, 75–85.
- (52) Loregian, A.; Rigatti, R.; Murphy, M.; Schievano, E.; Palù, G.; Marsden, H. S. Inhibition of human cytomegalovirus DNA polymerase by C-terminal peptides from the UL54 subunit. *J. Virol.* **2003**, *77*, 8336–8344.
- (53) Loregian, A.; Coen, D. M. Selective anti-cytomegalovirus compounds discovered by screening for inhibitors of subunit interactions of the viral polymerase. *Chem. Biol.* **2006**, *13*, 191–200.
- (54) Lin, M.; Tesconi, M.; Tischler, M. Use of ^1H NMR to facilitate solubility measurement for drug discovery compounds. *Int. J. Pharm.* **2009**, *369*, 47–52.
- (55) Kansy, M.; Senner, F.; Gubernator, K. Physicochemical high throughput screening: parallel artificial membrane permeation assay in the description of passive absorption processes. *J. Med. Chem.* **1998**, *41*, 1007–1010.
- (56) Cross, S.; Baroni, M.; Goracci, L.; Cruciani, G. GRID-based three-dimensional pharmacophores I: FLAPpharm, a novel approach for pharmacophore elucidation. *J. Chem. Inf. Model.* **2012**, *52*, 2587–2598.
- (57) Milletti, F.; Storch, L.; Sforza, G.; Cruciani, G. New and original pK_a prediction method using grid molecular interaction fields. *J. Chem. Inf. Model.* **2007**, *47*, 2172–2181.
- (58) Cruciani, G.; Milletti, F.; Storch, L.; Sforza, G.; Goracci, L. In silico pK_a prediction and ADME profiling. *Chem. Biodivers.* **2009**, *6*, 1812–1821.
- (59) Offermann, W.; Eger, K.; Roth, H. J. Synthesis of bicyclic 1,2,6-thiadiazines. *Arch. Pharm.* **1981**, *314*, 168–175.
- (60) Perrissin, M.; Favre, M.; Luu-Duc, C.; Bakri-Logeais, F.; Huguet, F.; Narcisse, G. Thieno[2,3-d]-4-pyrimidones: synthesis, structure and pharmacological properties. *Eur. J. Med. Chem.* **1984**, *19*, 420–424.
- (61) Loregian, A.; Appleton, B. A.; Hogle, J. M.; Coen, D. M. Residues of human cytomegalovirus DNA polymerase catalytic subunit UL54 that are necessary and sufficient for interaction with the accessory protein UL44. *J. Virol.* **2004**, *78*, 158–167.
- (62) Loregian, A.; Appleton, B. A.; Hogle, J. M.; Coen, D. M. Specific residues in the connector loop of the human cytomegalovirus DNA polymerase accessory protein, UL44, are crucial for interaction with the UL54 catalytic subunit. *J. Virol.* **2004**, *78*, 9084–9092.